

Calibration of phase-field brittle fatigue model by purposeful design of crack driving forces

K. Jukić^a, M. Ambati^b, T. Jarak^{a,c,*}, M. Kästner^d, Z. Tonković^a

^a Faculty of Mechanical Engineering and Naval Architecture, University of Zagreb, I. Lučića 5, 10000 Zagreb, Croatia

^b Material Mechanics and Durability, GE Global Research, 1 Research Circle, Niskayuna, NY 12309, USA

^c School of Industrial Engineering, University of Valladolid, Paseo del Cauce 59, 47011 Valladolid, Spain

^d Institute of Solid Mechanics, TU Dresden, 01062 Dresden, Germany

ARTICLE INFO

Keywords:

Phase-field
Fatigue
Calibration
Crack-driving forces

ABSTRACT

A new general multiparameter phase-field approach for high-cycle fatigue fracture is proposed. Fatigue is modelled by adding a new energy dissipation term accounting for fatigue phenomena, which results in two additional crack driving forces. The current model analysed in the paper possesses four fatigue parameters, whereby each of the driving forces depends on two parameters. The crack driving forces are designed so as to enable a more accurate reproduction of $S-N$ curves and the Paris' law by a single set of identified parameters, which is not possible by simpler phase-field models relying on only one or two fatigue parameters. The results indicate that the presented model is able to capture various macroscopic phenomena, including the mean stress effect, the evolution of complex crack patterns under cyclic loading and the reproduction of experimental $S-N$ and Paris curves of realistic materials. Extensive parametric analyses have revealed that there exists a strong correlation between the model fatigue parameters and the parameters defining $S-N$ and Paris' curves, which opens the possibility of straightforward calibration of each parameter from experimental data.

1. Introduction

Fatigue fracture is one of major engineering concerns in designing and maintaining structures and machine parts. The first recorded research of those phenomena, performed by Wöhler [1], was of a phenomenological and experimental nature. Later, Paris et al. [2] showed in their phenomenological studies, based on previous findings in fracture mechanics by Griffith [3] and Irwin [4,5], that there exists a certain connection between Griffith's and Wöhler's research when it comes to crack growth rates. Later, all these methods and resulting theories have been extended and improved, and even nowadays represent the basis for practical engineering fatigue failure analysis. However, precise tracking of crack initiation and propagation in realistic problems with complex loading and geometry is still a very challenging task, even when using sophisticated numerical methods [6]. Among them, in the last two decades, the Phase-Field (PF) method has proven to be a particularly promising approach. It is based on the variational approach to fracture proposed by Francfort and Marigo [7] and on a diffusive description of a crack (i.e., a diffusive description of a geometric discontinuity) inspired by the Ambrosio and Tortorelli approximation [8] of the Mumford-Shah functional [9]. Since its first application by Bourdin et al. [10], the method has gained enormous attention of the scientific community and has been extended to various fracture phenomena, mainly due to its elegance in resolving complex fracture problems, which follows only

* Corresponding author at: School of Industrial Engineering, University of Valladolid, Paseo del Cauce 59, 47011 Valladolid, Spain.
E-mail address: tomislav.jarak@uva.es (T. Jarak).

from solving a given set of partial differential equations without the need of any additional ad hoc criteria for crack initiation or propagation.

The topic of this paper is the modelling of fatigue fracture processes by the PF method, with special attention dedicated to reproducing classical phenomenological features, such as $S-N$ curves or the Paris law. Some of the first works to address fatigue modelling problems using the PF method [11,12] were based on extending the standard Ginzburg–Landau equation by appropriate additional terms that take into account fatigue effects in crack evolution. In [11,12] fatigue effects were modelled by adding new dissipation terms. On the other hand, in the early work [13] an additional internal fatigue variable was introduced, whose evolution is defined such that it preserves thermodynamical consistency. Again, an additional dissipation term associated with this independent variable appears in the phase-field evolution equation. However, although these formulations are clearly able to capture some fatigue failure phenomena, such as the total life dependent on a loading regime, it is not clear if they can realistically reproduce fatigue features such as $S-N$ curves or the Paris law. The first ones to reproduce the Wöhler's curves successfully were Alessi et al. [14]. They made the fracture toughness dependent on a history variable accounting for fatigue. That research was limited to the 1-D case and the fatigue history variable was defined as a time integral dependent on the strain. This approach was extended to 2D and 3D cases in Carrara et al. [15], where the fatigue history variable was assumed to be a time integral dependent on the tensile deformation energy density. The model naturally reproduced the $S-N$ and Paris' curves. In [16], Mesgarnejad et al. proposed two variations of their fatigue model, where either the entire fracture energy, or just its local term is degraded. As it has been demonstrated that the approach introduced in [15] is able to qualitatively reproduce both the crack growth laws and the stress-life approach, this strategy is at the moment widely adopted. It has also been extended to ductile fatigue by including various plasticity models [17–19]. In [17] plastic ratcheting was modelled, while in [18] fatigue was for the first time solved using an efficient monolithic solver based on the Broyden–Fletcher–Goldfarb–Shanno (BFGS) method. The model of Seleš et al. [19] was later used to study crack propagation at the microstructural level in [20]. On the other hand, Seiler et al. [21] utilised the local strain approach based on the Neuber rule to implicitly capture the effects of plastic deformation. Later, that model was used in [22] to take residual stresses into consideration. Hasan [23] utilised the concept to study the fatigue of brittle materials in a low-cycle regime. Therein, the evolution of the fatigue history variable might be affected by the rate of change of the standard history variable in such way that there is no accumulation of fatigue history variable in first cycle at all, leading to a model whose monotonic loading response is not affected by fatigue extension at all. Golahmar et al. [24] extended the fatigue approach based on the modification of fracture toughness to the hydrogen-assisted fatigue fracture by adding an additional fracture toughness modification function dependent on the hydrogen concentration, while in [25] an additional function describing martensitic phase transformations was utilised to study the fatigue behaviour of shape memory alloys. More recently, Alessi [26] extended Griffith's theory with the fracture toughness degradation concept, bridging the gap between phase-field fatigue models and Griffith's theory.

Besides the fracture toughness degradation concept, recently the models that increase the crack driving force have been proposed [27–30], motivated by early works [11–13]. Schreiber et al. [28] proposed a model with an additional fatigue potential that evolves following the Chaboche damage model. Among other fatigue phenomena, it allows the modelling of the mean stress effect. The additional fatigue potential leads to a new crack-driving force in the PF evolution equation, accounting for fatigue. However, this additional fatigue potential also produces an additional contribution in the definition of stress, whose satisfactory physical justification is at the moment still lacking, as it can make the material's response become (more or less) stiff during the fracture process. On the other hand, Loew et al. [27] studied the fatigue of rubber-like materials and defined an additional potential contribution that does not influence the stress definition. Lo et al. [29] utilised the micro-force balance, where they introduced a viscous term to model fatigue.

Despite the efficiency of the above-mentioned works resulted in models that possess the capability to reproduce basic fatigue features, it is not clear if any of them considers the fact that material degradation during crack initiation and crack propagation stages unfolds at different rates. As a result, it is unclear if crack initiation and crack propagation phenomena can be captured equally well by only one set of model parameters. Typically, in these models the same energetic quantity and parameters drive both fatigue crack initiation and fatigue crack propagation in the same way. Most models have only one or two material parameters for fatigue, which are usually used to describe both the Paris' law, describing the propagation of a well-defined crack, and the $S-N$ curves, where the crack initiation is always taken into account. This makes the classical fatigue material parameters strongly coupled in the existing PF fatigue models, complicating the model calibration procedure. A possible solution could be in defining more complex crack driving forces with extra parameters and with an appropriate dependence on the phase-field.

In this paper, a new PF model for brittle fatigue fracture is proposed, that can be calibrated to simultaneously reproduce a desired $S-N$ curve and a Paris' law. The model is based on adding an additional dissipative term to the total energy of a standard PF model for brittle fracture. Due to its simplicity, the well-known AT2 model for brittle fracture is considered in combination with the quadratic energy degradation function and the implicit enforcement of the phase field by the use of a history variable [31]. However, the proposed fatigue modelling could also be generalised to other similar models for brittle fracture. Newly added energy term results in two additional purposefully designed crack driving forces. Two fatigue history variables are introduced. The first one, called the fatigue crack initiation driving force, accumulates during the entire lifetime. It is dominantly responsible for the initiation of crack, but also slightly affects the crack propagation rate. The second fatigue history variable is called the fatigue crack propagation driving force. It accumulates only in the damaged state of material, i.e., in the crack propagation regime and strongly affects only crack propagation. Each history variable depends on two corresponding fatigue model parameters. Thereby, the parameters of the fatigue crack initiation driving force affect the crack initiation $S-N$ curve and set the lower bound on the crack growth rate, while the parameters of the fatigue crack propagation driving force are responsible primarily for the modification of the Paris' curve. In the limit case of a fast crack growth, when the total life is strongly dominated by crack initiation, the total

life $S-N$ curve is dominantly determined by the parameters of the fatigue crack initiation driving force. Furthermore, in each pair of parameters, one has a dominant effect on the empirical exponent of the corresponding experimental curve, while the other one is strongly associated with the curve coefficient. As a result, the calibration of the model is relatively simple and straightforward, because an initial guess for the values of model fatigue parameters can be deduced by inspecting either the experimental Paris' law or the $S-N$ curve.

The paper is organised as follows. In Section two, the AT2 model for brittle fracture under the assumption of small strains is described in the most important details in the quasi-static setting and then extended with fatigue capabilities. In Section three, the most important aspects of the numerical implementation of the model are given. In Section four, the results of numerical studies are presented, including the investigations of the studies about model parameters. At the end, in Section five the conclusions and lines for future research are proposed.

2. Phase-field approximation of fracture and fatigue

In this section, a fully calibratable PF model for fatigue fracture, based on an extension of the crack driving force, is proposed. Firstly, a PF model for quasi-static brittle fracture under small strain assumption, used for the development of the new fatigue model, is presented. Further, fatigue energetic quantities are defined and governing equations are derived.

2.1. Phase-field approximation of brittle fracture

The basis for most of PF models is the well established variational approach [7] to fracture which describes fracture as the minimisation of the total potential energy described by:

$$\Psi = \Psi_{\mathcal{E}} + \Psi_{\mathcal{f}} - \mathcal{P}, \quad (1)$$

where $\mathcal{P} = \mathcal{P}(\mathbf{u})$ is the external forces potential defined by:

$$\mathcal{P} = \int_{\Omega} \mathbf{b} \mathbf{u} \, dx + \int_{\Omega_B} \mathbf{t} \mathbf{u} \, dA, \quad (2)$$

with \mathbf{b} and \mathbf{t} as the body forces and surface tractions, respectively. Ω is a \mathcal{R}^N computational domain (body) and Ω_B is a \mathcal{R}^{N-1} boundary of the computational domain (the outer surface of the body).

The fracture energy is defined by:

$$\Psi_{\mathcal{f}} = \int_{\Omega} G_c \gamma \, dV, \quad (3)$$

where G_c is the critical energy release rate, and $\gamma = \gamma(\phi, \nabla\phi)$ is sometimes called the crack surface density function. The phase-field ϕ is bounded by 0 and 1, where 0 denotes healthy (intact) material and 1 corresponds to fully broken material. In Eq. (1), $\Psi_{\mathcal{E}} = \Psi_{\mathcal{E}}(\boldsymbol{\varepsilon}(\mathbf{u}))$ is the deformation energy, dependent on the small strain tensor $\boldsymbol{\varepsilon} = \frac{1}{2}(\nabla\mathbf{u} + (\nabla\mathbf{u})^T)$, with \mathbf{u} as the displacement field. As common in the PF methods, the stored energy is redefined as:

$$\Psi_{\mathcal{E}} = \int_{\Omega} \psi_{\mathcal{E}} \, dV, \quad \psi_{\mathcal{E}} = \psi_0^+ g + \psi_0^-, \quad (4)$$

where $\psi_{\mathcal{E}} = \psi_{\mathcal{E}}(\boldsymbol{\varepsilon}(\mathbf{u}), \phi)$ is the deformation energy density, $\psi_0^+ = \psi_0^+(\boldsymbol{\varepsilon}(\mathbf{u}))$ is the undegraded tensile part of the deformation energy density, $\psi_0^- = \psi_0^-(\boldsymbol{\varepsilon}(\mathbf{u}))$ is the compressive part of the deformation energy density and $g = g(\phi)$ is a monotonically decreasing function called the energy degradation function with the following properties: $g(0) = 1$ and $g(1) = 0$. The crack surface irreversibility writes:

$$\dot{\phi} \geq 0. \quad (5)$$

So far, various crack surface density functions, energy degradation functions and additive energy density decompositions have been proposed (see e.g., [32,33]). In this work, we limit our study to the well known AT2 model [10], which implies:

$$g = (1 - \phi)^2, \quad \gamma = \frac{1}{2} \left(\frac{1}{l} \phi^2 + l (\nabla\phi)^2 \right), \quad \varepsilon_{\text{crit}} = \sqrt{\frac{G_c}{3El}}, \quad \phi_{\text{crit}} = 0.25. \quad (6)$$

Herein, l stands for the length-scale parameter, which controls the diffusivity of the phase-field. Herein, $\varepsilon_{\text{crit}}$ and ϕ_{crit} denote the critical deformation and the critical phase-field, respectively, which correspond to the peak stress in the homogeneous one-dimensional (1-D) problem.

The deformation energy density used in this work is based on the often used spectral decompositions of strain tensor by Miehe [31] and Freddi [34].

2.2. Extension to fatigue

To adopt our PF model for fatigue analysis, we expand the fracture dissipation by an additional fatigue term, so that it is now written as:

$$\Psi_f = \Psi_{f,m} + \Psi_{f,c} = \int_{\Omega} G_c \gamma dV + \Psi_{f,c}, \quad (7)$$

where $\Psi_{f,m}$ is the part of fracture energy that is responsible for brittle fracture during monotonic loading, while the added term $\Psi_{f,c}$ is the dissipation due to fatigue (fracture caused by cyclic loading). The fatigue dissipation functional is defined as:

$$\Psi_{f,c} = \int_{\Omega} \int_0^{\tau} \frac{dg_{f,c}}{dt} (\psi_{\text{init}}(t) + \psi_{\text{prop}}(t)) dt dV, \quad (8)$$

where $\psi_{\text{init}} = \psi_{\text{init}}(t)$ is the term in the fatigue dissipation functional that drives fatigue crack initiation, and $\psi_{\text{prop}} = \psi_{\text{prop}}(t)$ is the part of fatigue dissipation potential that usually becomes dominant in fatigue crack propagation. The former contribution will be addressed as the fatigue crack initiation driving force, and the latter as the fatigue crack propagation driving force. The function $g_{f,c}$ defines how the accumulated fatigue driving forces influence the phase-field evolution. In general, different choices of $g_{f,c}$ can lead to different physical interpretations and models. In this work $g_{f,c} = g_{f,c}(\phi) = g(\phi)$ is proposed, which allows the interpretation of variables ψ_{init} and ψ_{prop} as “fatigue crack driving forces” and $g_{f,c}$ as the fatigue degradation function. Note that $g_{f,c} = g_{f,c}(\phi) = g(\phi)$ is used in the remainder of the text, including all simulations in Section 4, with the exception of Remark 3, where some other interesting choices are briefly discussed. Notion of $g_{f,c}(\phi)$ was used in the remainder of this section for sake of generality, except in Remark 3, where or $g_{f,c} = g_{f,c}(\phi, \nabla\phi)$ was introduced. The fatigue crack initiation and propagation driving forces are defined as:

$$\psi_{\text{init}}(\tau) = \psi_{\text{crit}}^{1-k_1} \int_0^{\tau} G_s k_3 H(\dot{\bar{\psi}}_{\text{init}}(t)) \dot{\bar{\psi}}_{\text{init}}(t) dt, \quad \bar{\psi}_{\text{init}} = (g^f \psi_0^+)^{k_1}, \quad (9)$$

$$\psi_{\text{prop}}(\tau) = \psi_{\text{crit}}^{1-k_2} \int_0^{\tau} F_s k_4 H(\dot{\bar{\psi}}_{\text{prop}}(t)) \dot{\bar{\psi}}_{\text{prop}}(t) dt, \quad \bar{\psi}_{\text{prop}} = (g^f \psi_0^+)^{k_2}, \quad (10)$$

where k_i , $i = 1, 2, 3, 4$ are the parameters of the model, H is the Heaviside function and G_s and F_s are the decoupling functions. The motivation for the definition of ψ_{init} is given in Section 4.2, where it is shown that Eq. (9) under some assumptions leads to a stress-life law that is equivalent to the Basquin's equation. This leads to simple physical interpretations of k_1 and k_3 parameters, and their clear correlation to the S - N curves, consequently leading to a simple calibration of these parameters. The definition of ψ_{prop} was motivated simply by favourable properties of the adopted ψ_{init} . It is to note that different definitions of $\bar{\psi}_{\text{init}} = \bar{\psi}_{\text{init}}((g^f \psi_0^+)^{k_1})$ and $\bar{\psi}_{\text{prop}} = \bar{\psi}_{\text{prop}}((g^f \psi_0^+)^{k_2})$ could be used for fine tuning of S - N curves and Paris' curves, but only Eqs. (9) and (10) are considered in this paper for the sake of simplicity. Additionally, it will be seen from the presented numerical results that under certain conditions the parameter k_1 is responsible for the exponent of crack initiation S - N curve, k_3 mostly affects the S - N curve coefficient, while k_2 and k_4 are associated with the exponent and coefficient of the Paris' curve, respectively. The premultiplication of integral terms by $\psi_{\text{crit}}^{1-k_1}$ and $\psi_{\text{crit}}^{1-k_2}$ makes the dimension of ψ_{init} and ψ_{prop} identical to the dimension of ψ . In this work, ψ_{crit} is defined by $\psi_{\text{crit}} = \frac{E}{2} \epsilon_{\text{crit}}^2$. The parameter f controls the influence of the fatigue crack driving forces on the localisation of phase-field and strains, and $f = 1$ was used in the remainder of the paper, unless explicitly stated otherwise.

Alternatively, ψ_{init} and ψ_{prop} could be written in a more general form:

$$\psi_{\text{init}} = \psi_{\text{crit}} D_{\text{init}} \left(\psi_{\text{crit}}^{-k_1} \int_0^{\tau} G_s k_3 H(\dot{\bar{\psi}}_{\text{init}}(t)) \dot{\bar{\psi}}_{\text{init}}(t) dt \right), \quad (11)$$

$$\psi_{\text{prop}} = \psi_{\text{crit}} D_{\text{prop}} \left(\psi_{\text{crit}}^{-k_2} \int_0^{\tau} F_s k_4 H(\dot{\bar{\psi}}_{\text{prop}}(t)) \dot{\bar{\psi}}_{\text{prop}}(t) dt \right), \quad (12)$$

where D_{init} and D_{prop} are arbitrary dimensionless monotonically increasing functions (with dimensionless arguments), that can be used to represent various damage accumulation laws. However, in the remainder of the work a simple forms $D_{\text{init}}(d_1) = d_1$ and $D_{\text{prop}}(d_2) = d_2$ are used, with:

$$d_1 = \psi_{\text{crit}}^{-k_1} \int_0^{\tau} G_s k_3 H(\dot{\bar{\psi}}_{\text{init}}(t)) \dot{\bar{\psi}}_{\text{init}}(t) dt, \quad (13)$$

$$d_2 = \psi_{\text{crit}}^{-k_2} \int_0^{\tau} F_s k_4 H(\dot{\bar{\psi}}_{\text{prop}}(t)) \dot{\bar{\psi}}_{\text{prop}}(t) dt. \quad (14)$$

Such choice corresponds to the definitions given in Eqs. (9) and (10). The notions of D_{init} and D_{prop} are not used in the rest of the work.

The functions G_s and F_s are used to decouple the crack initiation and the crack propagation behaviour. Setting $F_s(0) = 0$ reduces the influence of the fatigue crack propagation driving force on the crack initiation/growth for small phase-field values. In this work, the study is limited to the family of functions:

$$F_s = \begin{cases} 0, & \text{for } \phi < \phi_{\text{thres}} \\ \frac{\phi - \phi_{\text{thres}}}{1 - \phi_{\text{thres}}}, & \text{for } \phi \geq \phi_{\text{thres}} \end{cases} \quad (15)$$

where ϕ_{thres} is the threshold value of ϕ . The fatigue crack propagation driving force is not able to grow if ϕ is smaller than ϕ_{thres} . Physically justifiable alternative definitions of F_s could be $F_s(\psi_{\text{init}})$ and $F_s(\psi_{\text{init}}, \phi)$, but in this paper the presented study is limited to $F_s(\phi)$ only.

When it comes to the decoupling function G_s , it seems reasonable to define it as $G_s = 1 - F_s$, but, $G_s = 1$ is used in the presented study for the sake of simplicity. Note that although the function G_s could seemingly be used to achieve the complete decoupling of the fatigue crack driving forces, the crack initiation driving force could even in that case slightly influence the crack propagation rate, since it would keep accumulating in regions far away from the crack, where the values of the F_s would still be low. More optimal choices of G_s should be addressed in future research.

Remark 1. It should be noted that in the PF models based on additional fatigue dissipation contributions the evaluation of stress depends on the definition of these fatigue dissipation terms. If the stress is defined as the derivative of the total internal energy with respect to strains, $\sigma = \frac{d\psi_{\text{tot}}}{d\epsilon} = \frac{d\psi_{\text{el}}}{d\epsilon} + \frac{d\psi_{f,c}}{d\epsilon}$, it is clear that the second term is the contribution of fatigue dissipation to the stress. For example, fatigue dissipation can have a structure similar to that in [28]:

$$\Psi_{f,c} = \int_{\Omega} \psi_{f,c} dV, \quad \psi_{f,c} = g_{f,c} \psi_{\text{his}}, \tag{16}$$

with ψ_{his} as an arbitrary history variable defined in terms of strains and possibly some fatigue parameters, but independent of the phase field. Then it can be seen that:

$$\frac{d\psi_{f,c}}{d\epsilon} = g_{f,c} \frac{d\psi_{\text{his}}}{d\epsilon}, \tag{17}$$

is the nonzero contribution of the fatigue dissipation to the stress, which in [28] is attributed to micro-stresses caused by fatigue. However, in this work, the fatigue dissipation is defined as:

$$\Psi_{f,c} = \int_{\Omega} \int_0^{\tau} \frac{dg_{f,c}}{dt} \psi_{\text{his}}(t) dt dV = \int_{\Omega} \int_0^{\phi(\tau)} \frac{dg_{f,c}}{d\phi} \psi_{\text{his}}(\phi) d\phi dV, \tag{18}$$

which is equivalent to the definition in rate form, similar to the one used in [27]:

$$\dot{\Psi}_{f,c} = \int_{\Omega} \frac{dg_{f,c}}{dt} \psi_{\text{his}} dV = \int_{\Omega} \frac{dg_{f,c}}{d\phi} \psi_{\text{his}} \dot{\phi} dV. \tag{19}$$

The rate of the fatigue dissipation is then defined as:

$$\dot{\psi}_{f,c} = \frac{dg_{f,c}}{d\phi} \dot{\phi} \psi_{\text{his}}. \tag{20}$$

Note that according to the definition in Eq. (20), once when the fatigue process starts, $\psi_{\text{his}} > 0$. As ψ_{his} represents the fatigue driving forces accumulated in the material up to that moment, it can be regarded as a known constant value at current time step τ . It should be noted that ψ_{his} influences the change of the phase-field through the evolution equation (see Eqs. (29)–(30)). For small changes of time we can write:

$$d\psi_{f,c} = \frac{dg_{f,c}}{d\phi} \psi_{\text{his}} d\phi, \tag{21}$$

meaning that the fatigue dissipation density at some moment τ changes only due to the change of the phase-field, leading consequently to $\frac{d\psi_{f,c}}{d\epsilon} = 0$. It means that in the present model the stresses are calculated identically as in standard PF models for monotonous fracture. However, previous conclusion stands in the case of infinitesimal time step. For a finite time step size, newly obtained fatigue dissipation can be dependent on current displacement field, leading to possibility of additional stress term in discretised equations. This is discussed in Section 3.1 in detail.

Remark 2. Following the ideas from the previous remark, some comments regarding the models based on the degradation of fracture toughness can be given. The original model of Alessi et al. [14] (followed by [15]) gives the fracture energy by:

$$\Psi_f = \int_{\Omega} \psi_f dV, \quad \psi_f = \int_0^{\tau} \bar{F}(\psi_{\text{his}}) G_c \left(\frac{\partial \gamma}{\partial \phi} \dot{\phi} + \frac{\partial \gamma}{\partial (\nabla \phi)} (\nabla \dot{\phi}) \right) dt, \tag{22}$$

defining it as a path-dependent value, in contrast to the standard definition (3). Herein, the fatigue toughness degradation function $\bar{F}(\psi_{\text{his}})$ is the function of some arbitrary variable ψ_{his} that is dependent on the strain history and usually takes values between 1 for $\psi_{\text{his}} = 0$ and 0 for $\psi_{\text{his}} = \infty$. Again, using the argument that Ψ_f and ψ_f are constant for a fixed phase-field, one can conclude that $\frac{d\psi_f}{d\epsilon} = 0$, meaning that the extension to fatigue does not influence the stress definition.

However, most of other authors that use the fracture toughness degradation concept (such as [19,21,23–25]) define the fracture energy in the form of:

$$\Psi_f = \int_{\Omega} \bar{F}(\psi_{\text{his}}) G_c \gamma dV, \quad \psi_f = \bar{F}(\psi_{\text{his}}) G_c \gamma \tag{23}$$

which is clearly not equivalent to the original definition from [14,15]. Moreover, by seeking the derivative of ψ_f with respect to the strain tensor, one can get:

$$\frac{d\psi_f}{d\epsilon} = \frac{\partial \bar{F}(\psi_{\text{his}})}{\partial \psi_{\text{his}}} \frac{\partial \psi_{\text{his}}}{\partial \epsilon} G_c \gamma. \tag{24}$$

As the stress is defined for this type of model as $\sigma = \frac{d\psi_{tot}}{d\varepsilon} = \frac{d\psi_{\mathcal{E}}}{d\varepsilon} + \frac{d\psi_f}{d\varepsilon}$, it is clear that the term $\frac{\partial \overline{F}(\psi_{his})}{\partial \psi_{his}} \frac{\partial \psi_{his}}{\partial \varepsilon} G_c \gamma$ is the fatigue contribution to stress. In addition, the fracture energy defined by (23) contradicts thermodynamic requirements, as it can be reduced (due to the decreasing nature of $\overline{F}(\psi_{his})$) even if the constraint $\dot{\phi} \geq 0$ is always satisfied. To prove this claim, it is possible to consider a simple 1-D case with a homogeneous distribution of stress and phase-field, with the amplitude of stress such that it does not lead to a growth of phase-field in any moment and with a prescribed phase-field that is different from 0. Then, as loading cycles advance, the phase-field will remain constant, while the fatigue toughness degradation function will constantly decrease, leading to a decrease in the value of fracture dissipation potential.

2.3. Governing equations

Seeking the minima of Ψ in \mathbf{u} , and by recalling the definitions of \mathcal{P} , $\Psi_{\mathcal{E}}$ and $\sigma = \frac{\partial \psi_{\mathcal{E}}}{\partial \varepsilon} = g \frac{\partial \psi_0^+}{\partial \varepsilon} + \frac{\partial \psi_0^-}{\partial \varepsilon}$, one can obtain the natural boundary condition:

$$\mathbf{n}\sigma = \mathbf{t}, \quad \text{in } \Omega_N, \quad (25)$$

and the equilibrium equation:

$$\text{div} \sigma = -\mathbf{b}, \quad \text{in } \Omega, \quad (26)$$

as governing equations, where Ω_N is the part of Ω_B with the prescribed Neumann boundary conditions, while the Dirichlet boundary conditions are imposed on the rest of boundary Ω_B , denoted as Ω_D . Considering the constraints on ϕ (i.e., $\dot{\phi} \geq 0$), seeking the minima of Ψ in ϕ leads to:

$$\begin{aligned} \delta_{\phi} \Psi &= \int_{\Omega} \frac{dg}{d\phi} \psi_0^+ \delta\phi dV + \int_{\Omega} \frac{dg_{f,c}}{d\phi} (\psi_{\text{init}} + \psi_{\text{prop}}) \delta\phi dV \\ &+ \int_{\Omega} \left(\frac{\partial \gamma}{\partial \phi} G_c - \nabla \cdot \left(\frac{\partial \gamma}{\partial (\nabla \phi)} \right) G_c \right) \delta\phi dV + \int_{\Omega_B} \frac{\partial \gamma}{\partial (\nabla \phi)} \mathbf{n} G_c \delta\phi dA \geq 0 \end{aligned} \quad (27)$$

As customary, the homogeneous boundary conditions are adopted:

$$\frac{\partial \gamma}{\partial (\nabla \phi)} \mathbf{n} = 0, \quad \text{i.e. } \nabla \phi \cdot \mathbf{n} = 0, \quad \text{on } \Omega_B. \quad (28)$$

Finally, by adopting the special case $g_{f,c} = g$, and introducing (28) into the minimisation condition (27), and recalling the irreversibility condition of the phase-field and the energy conservation equation (see [33] for more details), we arrive to:

$$\frac{dg}{d\phi} (\psi_0^+ + \psi_{\text{init}} + \psi_{\text{prop}}) + \frac{\partial \gamma}{\partial \phi} G_c - \nabla \cdot \left(\frac{\partial \gamma}{\partial (\nabla \phi)} \right) G_c = 0, \quad \text{for } \dot{\phi} > 0, \quad (29)$$

$$\frac{dg}{d\phi} (\psi_0^+ + \psi_{\text{init}} + \psi_{\text{prop}}) + \frac{\partial \gamma}{\partial \phi} G_c - \nabla \cdot \left(\frac{\partial \gamma}{\partial (\nabla \phi)} \right) G_c \geq 0, \quad \text{for } \dot{\phi} = 0. \quad (30)$$

Now, note that $\frac{dg}{d\phi} (\psi_0^+ + \psi_{\text{init}} + \psi_{\text{prop}}) \leq 0$ because $\psi_0^+ + \psi_{\text{init}} + \psi_{\text{prop}} \geq 0$ and $\frac{dg}{d\phi} \leq 0$. Then, from Eqs. (29) and (30) and the definition of energetic quantities, by using the divergence theorem and the boundary conditions (28), one could derive:

$$\dot{\psi}_{f,m} \geq 0, \quad (31)$$

where $\dot{\psi}_{f,m}$ stands for the density of $\dot{\Psi}_{f,m}$, leading to the satisfaction of crack irreversibility (both locally and globally). In an analogous manner, considering the fact that $\frac{dg}{d\phi} \psi_0^+ \leq 0$, one could derive:

$$p - \dot{\psi}_{\mathcal{E}} = \dot{d} = \dot{\psi}_{f,m} + \dot{\psi}_{f,c} \geq 0, \quad (32)$$

with p being the density of internal power and with \dot{d} being the density of dissipation rate, showing that the second law of thermodynamics (dissipation inequality) is satisfied.

However, to simplify the irreversibility enforcement, in this work we use the history field concept by Miehe [31], which modifies Eqs. (29) and (30) into:

$$\frac{dg}{d\phi} (H + \psi_{\text{init}} + \psi_{\text{prop}}) + \frac{\partial \gamma}{\partial \phi} G_c - \nabla \cdot \left(\frac{\partial \gamma}{\partial (\nabla \phi)} \right) G_c = 0. \quad (33)$$

Herein, the history field H is defined as:

$$H(t) = \min_{\tau \in [0,t]} (\psi_0^+(\tau)). \quad (34)$$

Remark 3. The choice of the function $g_{f,c}$ in the proposed framework leads to different fatigue PF models. Theoretically, different forms of the function are allowed, including either $g_{f,c} = g_{f,c}(\phi)$ or $g_{f,c} = g_{f,c}(\phi, \nabla \phi)$. In general, the function $g_{f,c}$ should be defined such that $\frac{dg_{f,c}}{d\phi} \dot{\phi} \leq 0$ stands. As a consequence, fatigue encourages the growth of phase-field and therefore simulates damage due to

fatigue. In the following text, two alternative definitions of $g_{f,c}$ are considered. An interesting choice for the function depending on the phase-field gradient is:

$$g_{f,c} = g_{f,c}(\phi, \nabla\phi) = -\gamma(\phi, \nabla\phi), \quad (35)$$

which results in a model based on the fracture toughness degradation concept. By using Eq. (35), and by taking derivative of Eq. (8), the fatigue dissipation rate is:

$$\dot{\psi}_{f,c} = \int_{\Omega} \frac{dg_{f,c}}{dt} (\psi_{init} + \psi_{prop}) dV = \int_{\Omega} -\frac{d\gamma}{dt} (\psi_{init} + \psi_{prop}) dV = \int_{\Omega} -\left(\frac{\partial\gamma}{\partial\phi}\phi + \frac{\partial\gamma}{\partial(\nabla\phi)}(\nabla\phi)\right) (\psi_{init} + \psi_{prop}) dV \quad (36)$$

and the total dissipation rate obtains the following form:

$$\dot{\psi}_f = \int_{\Omega} \frac{d\gamma}{dt} G_c dV + \int_{\Omega} \frac{dg_{f,c}}{dt} (\psi_{init} + \psi_{prop}) dV = \int_{\Omega} \frac{d\gamma}{dt} (G_c - \psi_{init} - \psi_{prop}) dV. \quad (37)$$

The variables ψ_{init} and ψ_{prop} as proposed by Eqs. (9)–(14) can be regarded as the fatigue history variables, noted here as $\psi_{init} = \alpha_1$ and $\psi_{prop} = \alpha_2$. Then, after some simple manipulation, the dissipation rate (37) can be written as:

$$\dot{\psi}_f = \int_{\Omega} \frac{d\gamma}{dt} G_c \bar{F}_1(\alpha_1, \alpha_2) dV, \quad (38)$$

where $\bar{F}_1(\alpha_1, \alpha_2)$ is function of internal variables:

$$\bar{F}_1 = 1 - \frac{\alpha_1 + \alpha_2}{G_c} = 1 - \frac{\psi_{init} + \psi_{prop}}{G_c}, \quad (39)$$

with ψ_{init} and ψ_{prop} such that $0 \leq \psi_{init} + \psi_{prop} \leq G_c$ throughout of the process. The closer inspection reveals that Eq. (38) corresponds exactly to the definition of the fracture energy proposed in Carrara et al. [15], meaning that this choice yields a PF model based on the fracture toughness degradation. Note that in the corresponding literature the function \bar{F}_1 is called the fatigue degradation function, rather than $g_{f,c}$. This means that this model belongs to the group of fatigue PF models based on the degradation of fracture toughness, see e.g. [14,15].

The corresponding phase-field evolution equation is:

$$\frac{dg}{d\phi} \mathcal{H} + \frac{\partial\gamma}{\partial\phi} \bar{F}_1 G_c - \nabla \cdot \left(\frac{\partial\gamma}{\partial(\nabla\phi)}\right) \bar{F}_1 G_c - \frac{\partial\gamma}{\partial(\nabla\phi)} \cdot \nabla \bar{F}_1 G_c = 0. \quad (40)$$

which is again equivalent to one in [15], but with \bar{F}_1 as the fatigue degradation function dependent of two fatigue history variables.

If the function $g_{f,c}$ is chosen to depend only on the phase field, $g_{f,c} = g_{f,c}(\phi)$, then the fatigue dissipation rate becomes:

$$\dot{\psi}_{f,c} = \int_{\Omega} \frac{dg_{f,c}}{dt} (\psi_{init} + \psi_{prop}) dV = \int_{\Omega} \frac{dg}{dt} (\psi_{init} + \psi_{prop}) dV \quad (41)$$

and the corresponding phase-field evolution equations are:

$$\frac{dg}{d\phi} \mathcal{H} + \frac{dg_{f,c}}{d\phi} (\psi_{init} + \psi_{prop}) + \frac{\partial\gamma}{\partial\phi} G_c - \nabla \cdot \left(\frac{\partial\gamma}{\partial(\nabla\phi)}\right) G_c = 0. \quad (42)$$

For the particular choice used in this article, $g_{f,c} = g$, it has been shown in Section 2.3. that ψ_{init} and ψ_{prop} can be regarded as fatigue crack driving forces. Alternatively, choice $g_{f,c} = g$ can be disregarded, and $g_{f,c}$ can be defined such that:

$$\frac{dg_{f,c}}{d\phi} = -k \frac{\partial g_{f,c}}{\partial\phi} \quad (43)$$

with $k > 0$, where k is introduced for the sake of normisation of $g_{f,c}$. By applying the function (43) to define the fatigue dissipation rate, the phase field evolution (42) can be rewritten as:

$$\frac{dg}{d\phi} \mathcal{H} + \frac{\partial\gamma}{\partial\phi} \bar{F}_2 G_c - \nabla \cdot \left(\frac{\partial\gamma}{\partial(\nabla\phi)}\right) G_c = 0, \quad (44)$$

with:

$$\bar{F}_2 = 1 - \frac{\alpha_1 + \alpha_2}{G_c} = 1 - \frac{\psi_{init} + \psi_{prop}}{G_c}, \quad (45)$$

which is to some extent similar to a model that can be found in work of Mesgarnejad et al. [16]. Note that ψ_{init} and ψ_{prop} should now be defined such that $k(\psi_{init} + \psi_{prop}) \leq G_c$. By using the usual second order form of γ , $\gamma = \frac{1}{c} \left(\frac{1}{l} \beta(\phi) + l(\nabla\phi)^2\right)$, by introducing the variables $(G_c)_{eff} = \sqrt{\bar{F}_2} G_c$ and $l_{eff} = \frac{G_c}{\sqrt{\bar{F}_2}}$ and utilising them in Eq. (44) we finally obtain:

$$\frac{dg}{d\phi} \mathcal{H} + \frac{\partial\beta}{\partial\phi} \frac{(G_c)_{eff}}{l_{eff}^c} - \nabla \cdot \nabla\phi \frac{2l_{eff}(G_c)_{eff}}{c} = 0, \quad (46)$$

Since $(G_c)_{\text{eff}} \leq G_c$ and $l_{\text{eff}} \geq l$, we can conclude with certainty that in this model the fatigue will lead to the widening of the localisation zone. Note that for this state the fatigue dissipation reduces only the local resistance to crack growth (similar to one model defined in [16]). Although this analysis and conclusion are not directly applicable to the model with $g_{f,c} = g$ used in the rest of the paper, it can serve to better understand the widening of the PF profile observed in the results presented in Section 4.

3. Numerical implementation

In this section the numerical implementation of the proposed fatigue model is briefly described, including the time integration of dissipation potentials and the employed cycle skipping procedure. For completeness, some information about the discretisation and the staggered solver is also included.

3.1. Time integration of $\psi_{f,c}$

To derive discretised equations by using the virtual work principle, which is described in the next subsection, it is necessary to define all energetic quantities in given time step. As fatigue dissipation is actually a path-dependent, it is necessary to properly discretise it in time. Motivated by the definition from Eq. (8) and the discussion from Remark 1, we assume:

$$\psi_{f,c}(\tau + \Delta\tau) = \psi_{f,c}(\tau) + \int_{\tau}^{\tau+\Delta\tau} \frac{dg_{f,c}}{dt} (\psi_{\text{init}} + \psi_{\text{prop}}) dt = \psi_{f,c}(\tau) + \Delta\psi_{f,c}, \quad (47)$$

where the increment term $\Delta\psi_{f,c}$ is approximated by a simple scheme, as:

$$\Delta\psi_{f,c} \approx \Delta g_{f,c} (\psi_{\text{init}}(\tau) + \psi_{\text{prop}}(\tau)) = (g_{f,c}(\tau + \Delta\tau) - g_{f,c}(\tau)) (\psi_{\text{init}}(\tau) + \psi_{\text{prop}}(\tau)), \quad (48)$$

which is fully consistent with the governing equations given in Section 2.3 and the definition of stress discussed in Remark 1, $\sigma = \frac{d\psi_{f,c}}{d\varepsilon}$ (i.e., $\frac{d\psi_{f,c}(\tau+\Delta\tau)}{d\varepsilon(\tau+\Delta\tau)} = 0$). The term $\Delta\psi_{f,c}$ manifests only as new crack driving forces in the discretised phase-field equation (see Eq. (53)) that depends on frozen value of the fatigue crack driving forces ψ_{init} and ψ_{prop} . Consequently, the crack driving force can be integrated at the end of an increment.

Alternatively, $\Delta\psi_{f,c}$ could be defined as:

$$\Delta\psi_{f,c} \approx (g_{f,c}(\tau + \Delta\tau) - g_{f,c}(\tau)) (\psi_{\text{init}}(\tau + \Delta\tau) + \psi_{\text{prop}}(\tau + \Delta\tau)). \quad (49)$$

However, in this case, $\psi_{\text{init}}(\tau + \Delta\tau)$ and $\psi_{\text{prop}}(\tau + \Delta\tau)$, are dependent on new strains and PF, and new nonlinear terms that contain $\Delta g_{f,c} \left(\frac{d\psi_{\text{init}}}{d\varepsilon} + \frac{d\psi_{\text{prop}}}{d\varepsilon} \right)$ and $\Delta g_{f,c} \left(\frac{d\psi_{\text{init}}}{d\phi} + \frac{d\psi_{\text{prop}}}{d\phi} \right)$ would appear in the discretised phase-field equations. In addition, unlike definition by Eq. (48), definition by Eq. (49) can be nonconvex in ε , which is undesirable. Also, note that for sufficiently small time step or a small load increment, the value of $\Delta g_{f,c}$ will be very small, and consequently, new terms can be simply disregarded in most of situations. As the matter of fact, these conclusions hold for any scheme that use ψ_{init} and ψ_{prop} values from $\tau + \Delta\tau$ time step.

In this paper, we use the fatigue crack driving forces from new time step $\tau + \Delta\tau$ (assumption of Eq. (49)). However, we disregarded the fact that new fatigue crack driving force depends on new values of strains and phase-field. Consequently, all possible new terms in discretised equations that depend on $\Delta g_{f,c}$ are disregarded. As result, only new terms that can be found in discretised phase-field Eq. (53) are $\frac{dg}{d\phi} (\psi_{\text{init}}(\tau + \Delta\tau) + \psi_{\text{prop}}(\tau + \Delta\tau))$ and $\frac{d^2g}{d\phi^2} (\psi_{\text{init}}(\tau + \Delta\tau) + \psi_{\text{prop}}(\tau + \Delta\tau))$. Authors are aware that this could be inconsistent with previous analysis, and that this could be seen as inaccuracy, but this simplification barely influences the final results. This is corroborated by fact that fatigue evolves slowly within large number of cycles and load increments. In the presented numerical analyses each load cycle is subdivided in 10 uniform load increments, which is by author experience sufficient to properly capture evolution of phase-field and fatigue variables. In addition, convergence issues were not experienced.

Note that the analysis presented above is applicable to the arbitrary choice of $g_{f,c}$ including those that lead to model based on concept of fracture toughness degradation.

3.2. FEM discretisation

The virtual work principle is used to develop the discretised set of equations in the Finite Element Method (FEM) framework. At the global level, displacement and phase-field are interpolated using nodal values as:

$$\mathbf{u} = \mathbf{N}_u^T \mathbf{v}, \quad \phi = \mathbf{N}_\phi^T \phi_n, \quad (50)$$

where \mathbf{N}_u and \mathbf{N}_ϕ stand for matrices of shape functions for displacement and phase-field, respectively, while \mathbf{v} are nodal displacements and ϕ_n are nodal phase-field values. Strains and phase-field gradients are written in the matrix form as:

$$\boldsymbol{\varepsilon} = \mathbf{B}_u^T \mathbf{v}, \quad \nabla\phi = \mathbf{B}_\phi^T \phi_n, \quad (51)$$

where \mathbf{B}_u and \mathbf{B}_ϕ are matrices that at the global level relate nodal displacements to strains, and the nodal phase-field values to the phase-field gradient, respectively. In this work, both the phase field and displacements are discretised by using the first-order isoparametric quadrilateral elements with the bilinear field distribution. The discretised equations are derived by imposing the

equality variational minimisation condition on the functional, which after employing the approximations of field variables (50)–(51), and performing linearisation yield the following discretised equations:

$$\left(\int_{\Omega} \mathbf{B}_u \frac{\partial \boldsymbol{\sigma}}{\partial \boldsymbol{\epsilon}} \mathbf{B}_u^T dV \right) \Delta \mathbf{v} = - \int_{\Omega} \mathbf{B}_u \boldsymbol{\sigma} dV + \int_{\Omega} \mathbf{N}_u \mathbf{b} dV + \int_{\Omega_N} \mathbf{N}_u \mathbf{t} dA. \quad (52)$$

and:

$$\begin{aligned} & \left(\int_{\Omega} \left(\mathbf{N}_{\phi} \left(G_c \frac{\partial^2 \gamma}{\partial \phi^2} + \frac{d^2 g}{d\phi^2} (\psi_0^+ + \psi_{\text{init}} + \psi_{\text{prop}}) \right) \mathbf{N}_{\phi}^T + G_c \mathbf{B}_{\phi} \frac{\partial^2 \gamma}{\partial (\nabla \phi)^2} \mathbf{B}_{\phi}^T \right) dV \right) \Delta \phi_n \\ & = - \int_{\Omega} \left(\mathbf{N}_{\phi} \left(G_c \frac{\partial \gamma}{\partial \phi} + \frac{dg}{d\phi} (\psi_0^+ + \psi_{\text{init}} + \psi_{\text{prop}}) \right) + G_c \mathbf{B}_{\phi} \frac{\partial \gamma}{\partial (\nabla \phi)} \right) dV \end{aligned} \quad (53)$$

3.3. Solver procedure

A multi-pass staggered solver with convergence control is used to solve phase-field fatigue problems. Within one iteration of a staggered algorithm, first the displacement problem is solved using the Newton’s algorithm, and then the phase-field problem is solved with the newly obtained displacement. Time integration is done after the solving of phase-field problem. At the end of staggered iteration, the residual is checked, and a new increment starts if the residual is smaller than predefined tolerance. The residual is defined as the quadratic norm of residual vector for the displacement problem, and it is calculated after solving phase-field problem. Load cycles are divided in uniform increments. After every three load cycles, cycle skipping, described in Section 3.5, is performed.

3.4. Time integration of history variables

Since in this work the fatigue initiation and propagation driving forces are defined as time integrals, one has to integrate them within each increment. The fatigue crack driving forces are integrated as:

$$\begin{aligned} \psi_{\text{init}}(\tau + \Delta\tau) &= \psi_{\text{init}}(\tau) + \psi_{\text{crit}}^{(1-k_1)} k_3 \text{H} \left(g(\phi(\tau + \Delta\tau))^f \psi_0^+(\tau + \Delta\tau) - g(\phi(\tau))^f \psi_0^+(\tau) \right) \\ & \quad \left(\left(g(\phi(\tau + \Delta\tau))^f \psi_0^+(\tau + \Delta\tau) \right)^{k_1} - \left(g(\phi(\tau))^f \psi_0^+(\tau) \right)^{k_1} \right). \end{aligned} \quad (54)$$

$$\begin{aligned} \psi_{\text{prop}}(\tau + \Delta\tau) &= \psi_{\text{prop}}(\tau) + \psi_{\text{crit}}^{(1-k_2)} k_4 \text{H} \left(g(\phi(\tau + \Delta\tau))^f \psi_0^+(\tau + \Delta\tau) - g(\phi(\tau))^f \psi_0^+(\tau) \right) \\ & \quad \frac{F(\phi(\tau + \Delta\tau)) + F(\phi(\tau))}{2} \left(\left(g(\phi(\tau + \Delta\tau))^f \psi_0^+(\tau + \Delta\tau) \right)^{k_2} - \left(g(\phi(\tau))^f \psi_0^+(\tau) \right)^{k_2} \right). \end{aligned} \quad (55)$$

3.5. Cycle skipping

In order to speed up the calculations, in this work we apply an adaptation of cycle skipping originally proposed by Cojocaru and Karlsson [35]. Similar cycle skipping was used in phase-field fatigue modelling [19,27]. In contrast to [19,27,35], in the current adaptation the admissible number of skipped cycles is calculated for both extrapolated fields (fatigue driving forces), and the lower obtained number is chosen for extrapolation.

During cycle skipping, the fatigue driving forces are extrapolated in each integration point by using data from previous three successive load cycles as:

$$\psi_{\text{init,ext}} = \psi_{\text{init}} + \Delta_{2-3} \psi_{\text{init}} N_{\text{skip}} + \frac{\Delta_{2-3} \psi_{\text{init}} - \Delta_{1-2} \psi_{\text{init}}}{2} N_{\text{skip}}^2, \quad (56)$$

where $\psi_{\text{init,ext}}$ stands for the extrapolated fatigue crack initiation driving force, $\Delta_{j-k} \psi_{\text{init}} = \psi_{\text{init}}(N_{k+j-1}) - \psi_{\text{init}}(N_{k+i-1})$ stands for the change of fatigue crack initiation driving force between i th and j th cycle in the set of previous three successive cycles, k is the index of the first cycle in set of three cycles that are taken into account for cycle skipping, $\psi_{\text{init}}(N_i)$ is value of fatigue crack initiation driving forces at end of i th loading cycle and N_{skip} stands for a number of skipped cycles. The extrapolated propagation driving force is calculated analogously to the extrapolated initiation driving force. The number of skipped cycles is calculated as:

$$n_{\text{skip}} = \min_i \left(\min \left(\left| \frac{\Delta_{2-3} \psi_{\text{init},i}}{\Delta_{2-3} \psi_{\text{init},i} - \Delta_{1-2} \psi_{\text{init},i}} \right|, \left| \frac{\Delta_{2-3} \psi_{\text{prop},i}}{\Delta_{2-3} \psi_{\text{prop},i} - \Delta_{1-2} \psi_{\text{prop},i}} \right| \right) \right), \quad (57)$$

$$N_{\text{skip}} = \min \left(\max \left(\text{tol} \cdot n_{\text{skip}}, N_{\text{min}} \right), N_{\text{max}} \right), \quad (58)$$

where n_{skip} is calculated by considering data from all integration points, and where the index i identifies the integration point of FE model, $\Delta_{j-k} \psi_{\text{prop},i}$ stands for the change of propagation dissipation potential density between the j th and the k th cycle, tol is a prescribed value, while N_{min} and N_{max} are the prescribed minimal and maximal allowed number of skipped cycles.

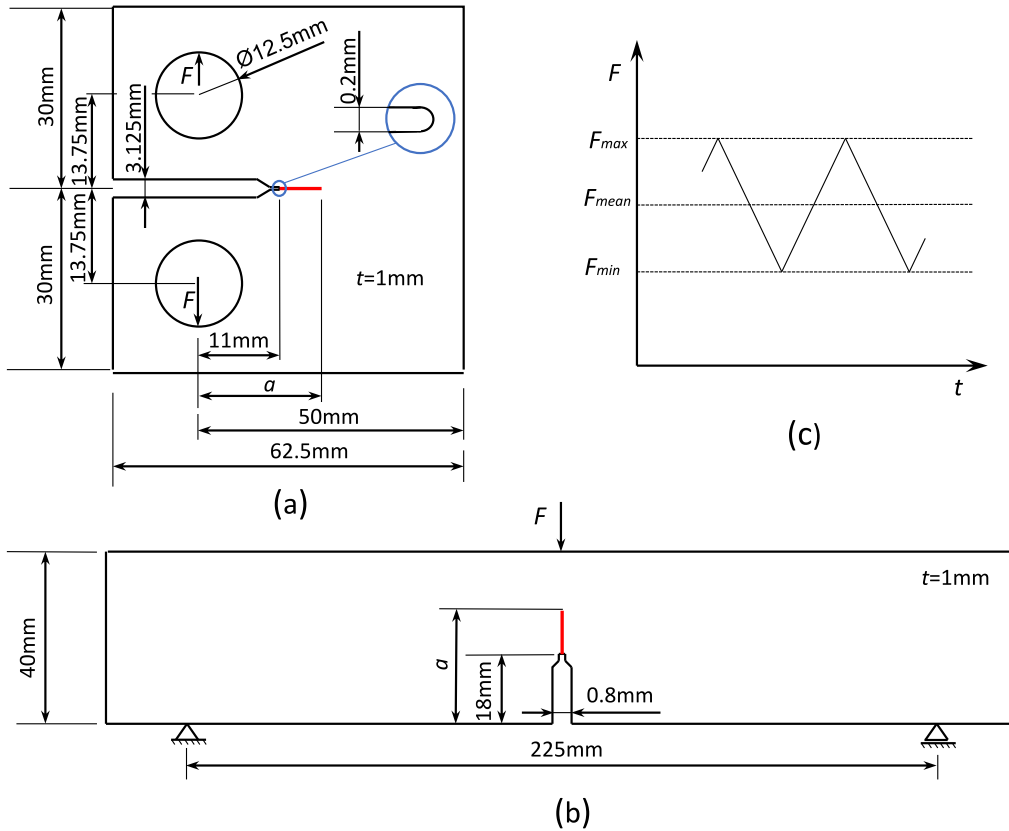


Fig. 1. Geometry, loads and boundary conditions for compact tension specimen (a), three point bending test specimen (b), and loading cycle description (c).

4. Results and discussion

4.1. Studied examples and simulation settings

In this subsection, the geometry, loading and boundary conditions of the considered problems are described. In the presented simulations, a compact tension specimen (CT specimen) or a three point bending specimen (TPB specimen) are used, whose geometries are shown in Fig. 1a and b, respectively. Additional Dirichlet boundary conditions on the phase-field ($\phi = 0$) are prescribed around points with applied loads or displacements, with the goal of avoiding initiation of cracks at those points. An exemplary loading cycle is shown in Fig. 1c, and in most examples cycles with $F_{min} = 0$ are used. Therefore, the ordinate in the shown $S-N$ diagrams will represent both maximal force and force range, and is denoted simply as F . The only exception are examples where the mean stress or the loading ratio effect is studied (see Section 4.3). The used model parameters are $k_1 = 2$, $k_2 = 1$, $k_3 = 0.001$, $k_4 = 1$ and $\phi_{thres} = 0.4$, unless specified otherwise. These values are also used as default parameters in parametric studies. Such choice of default parameters will give a reasonable number of cycles for the studied force ranges in both the crack initiation and the crack propagation regime, leading to reasonable computational costs. The model parameters are varied in Section 4.2, where each parameter is varied individually, and its influence is studied. The applied mesh size is $h \approx \frac{l}{6}$ in most simulations, but the effect of mesh size is demonstrated in Section 4.5.2. Used cycle skipping tolerance is 0.01. Cycles in simulations are divided in 10 increments. The applied material parameters are $E = 116000\text{MPa}$, $\nu = 0.33$, $G_c = 35.31\text{MPa mm}$, $\sigma_{crit} = 970\text{MPa}$, leading to $l = 0.4582\text{mm}$ for the AT2 model. In all considered cases, plane stress state is assumed, and Miehe's split is used, except for example in Section 4.5.5, where Freddi's split and a hybrid approach are used. In most simulations, the observed quantities are the crack initiation life, the total life and crack growth rates. The crack length is determined by tracking maximum coordinates of nodes with phase-field values higher than 0.95, and consequently, the crack is considered initiated when the nodal phase-field value reaches the value of 0.95. $\frac{da}{dN}$ is calculated as $\frac{\Delta a}{\Delta N}$ at a moment of change of the crack length. A specimen is considered fully fractured when the total crack length reaches a value close to 45 mm for the CT specimen and 35 mm for the TPB specimen. Stress intensity factors used for $\frac{da}{dN} - \Delta K$ plots are calculated from:

$$K = \sigma I \sqrt{\pi a}, \quad (59)$$

where I stands for the coefficient dependent on crack length and geometry, whose values can be found in [36]. In most results that include S - N curves, two different types of S - N curves are displayed. The first one has the structural life (given by the number of cycles N) defined as the total number of cycles to complete failure and is called the total life S - N curve in text. The other type uses the number of cycles to crack (damage) initiation and is called the initiation S - N curve. Thereby, the crack initiation is defined by the cycle where the phase-field value of 0.95 is observed for the first time.

4.2. Influence of model parameters

In this subsection, we aim to demonstrate the effect of model parameters on the resulting fatigue behaviour. The main goal is to reproduce the S - N curve and Paris' curves. Accordingly, the total life in the high-cycle fatigue regime has to be described by:

$$\sigma = AN^\beta, \quad (60)$$

and the crack growth rate by:

$$\frac{da}{dN} = C(\Delta K)^m, \quad (61)$$

where A and β are the coefficient and exponent of the S - N curve, respectively, while C and m are the Paris' curve coefficient and exponent, respectively. To predict the model behaviour prior to performing expensive numerical experiments, one can assume a simple 1-D 'crack initiation' case with homogeneous stress and phase-field distributions. All loading cycles are identical, with $\sigma_{\min} = 0$ and $\sigma_{\max} = \sigma < \sigma_{\text{crit}}$, where σ_{crit} is the peak stress for the 1-D stress state (usually equal to the tensile strength). Accordingly, the growth of the fatigue initiation driving force during one cycle is given by:

$$\psi_{\text{init},1} = \psi_{\text{crit}}^{1-k_1} k_3 (g^f \psi_0^+)^{k_1} = \psi_{\text{crit}}^{1-k_1} k_3 \left(g^f \frac{\sigma^2}{g^2 E} \right)^{k_1}. \quad (62)$$

Further, for simplicity of this discussion, we choose $f = 2$ and we assume that the tensile deformation energy density is much smaller than the accumulated fatigue driving force. Then, we assume that the damage initiation occurs when $N \cdot \psi_{\text{init},1}$ reaches some critical value $\psi_{\text{crit,init}}$:

$$N \psi_{\text{crit}}^{1-k_1} \frac{k_3}{E^{k_1}} (\sigma)^{2k_1} = \psi_{\text{crit,init}}. \quad (63)$$

By algebraic manipulation, one can get to:

$$\sigma = (k_3 N)^{-\frac{1}{2k_1}} \cdot \text{Const} = N^\beta A, \quad (64)$$

leading to the conclusion that the proposed model reproduces the initiation S - N curve naturally with $\beta = -\frac{1}{2k_1}$ and $A = \text{Const} \cdot k_3^\beta$. The result $\beta = -\frac{1}{2k_1}$ directly leads to the initial assumption regarding the calibration of the slope of S - N curve. This is confirmed by numerical simulations and shown in Fig. 2. In addition, by manipulating Eq. (64), one can get:

$$N = \frac{1}{k_3} \left(\frac{\sigma}{\text{Const}} \right)^{-2k_1}, \quad (65)$$

leading to the conclusion that $k_3 N$ is constant for fixed σ , consequently leading to the conclusion that k_3 scales calculated cycles, as well as the S - N curve coefficient, in linear manner. This can also be confirmed by numerical simulation, as shown in Fig. 3.

Although in the previous analysis the fatigue crack driving force was neglected, the results in Figs. 2 and 3, demonstrate that the above conclusions are valid even for numerical simulations with the fatigue crack propagation driving force being included. When it comes to the influence of k_1 parameter, in case of the crack initiation S - N curve, relation between k_1 and the curve's slope indeed can be approximated by term $\beta = -\frac{1}{2k_1}$ as predicted above and shown in Fig. 2d. The total life S - N curve is influenced by both the crack initiation and the crack propagation time, and therefore the slope of this curve will also be influenced by the crack propagation driving force and all k_i parameters. Nevertheless, the relation between the total life S - N curve's parameters and the k_1 parameter is still almost linear (see Fig. 2d), which is beneficial for simplicity of calibration process. In addition, it should be noted that as the k_1 parameter is increased, rate of accumulation of crack initiation driving force in a single cycle decreases for low values of $\bar{\psi}_{\text{init}}$, while rate of accumulation of crack initiation driving force increases for values of $\bar{\psi}_{\text{init}}$ that are higher than ψ_{crit} (see Eqs. (9) and (10)), leading to the smaller initiation and total number of cycles in low-cycle fatigue regime and higher number of cycles in high-cycle fatigue regime (see Fig. 2a and b). Furthermore, it should be noted that with lowering the maximum load the obtained total-life S - N curves seem to converge to linear curves (in the logarithmic scale). Theoretically, the total life curve could possibly be bilinear in the high-cycle fatigue regime. This can occur when propagation life is dominant for high loads and initiation life is dominant for small loads, or vice versa. However, these phenomena have not been captured in any of the presented numerical analyses. In addition, note that in the present model the cut off due to the endurance limit is not explicitly modelled, and this issue is outside of the scope of this article.

Prior to discussion on k_1 influence on Paris' curve, it should be noted that the crack initiation driving force, unlike the crack propagation driving force, accumulates through whole lifetime. Therefore, it influences both crack initiation and propagation, and actually sets the lower bound on the crack growth rate. However, the intensity of influence during the crack initiation and the crack propagation stage can be discussed. Clearly, as the crack propagation driving force starts to accumulate only when the phase-field

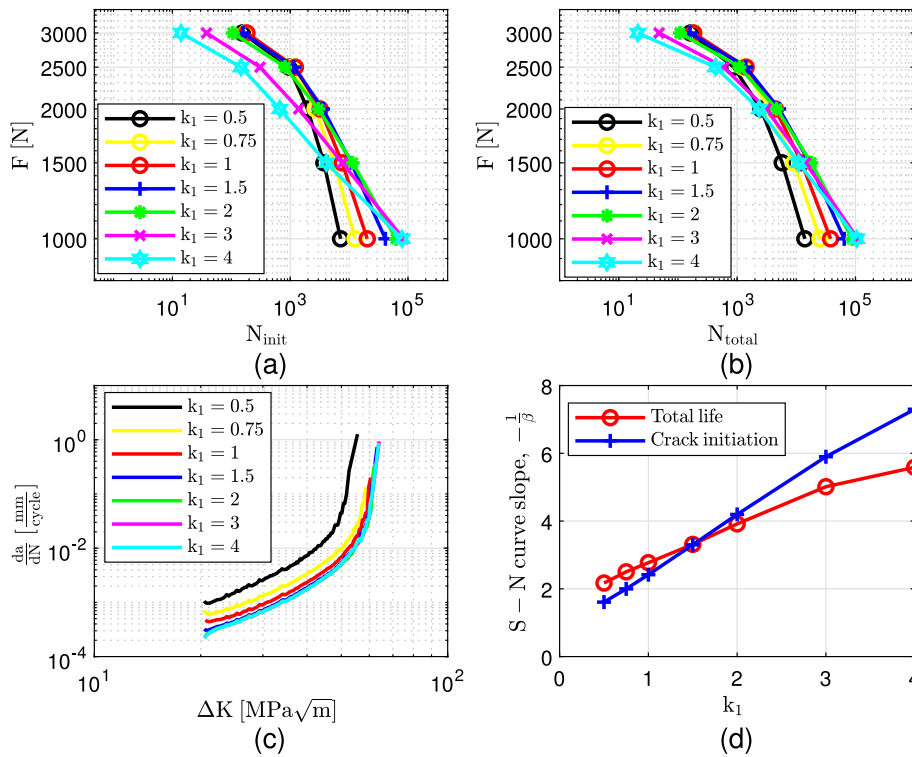


Fig. 2. Influence of k_1 parameter. Initiation $S-N$ curves (a), total life $S-N$ curves (b), Paris' curves for $F = 1000$ N (c) and relation between k_1 and $-\frac{1}{\beta}$ (d) for different values of k_1 . Parameter β is calculated as slope of $S-N$ curve between points with $F = 1500$ N and $F = 1000$ N.

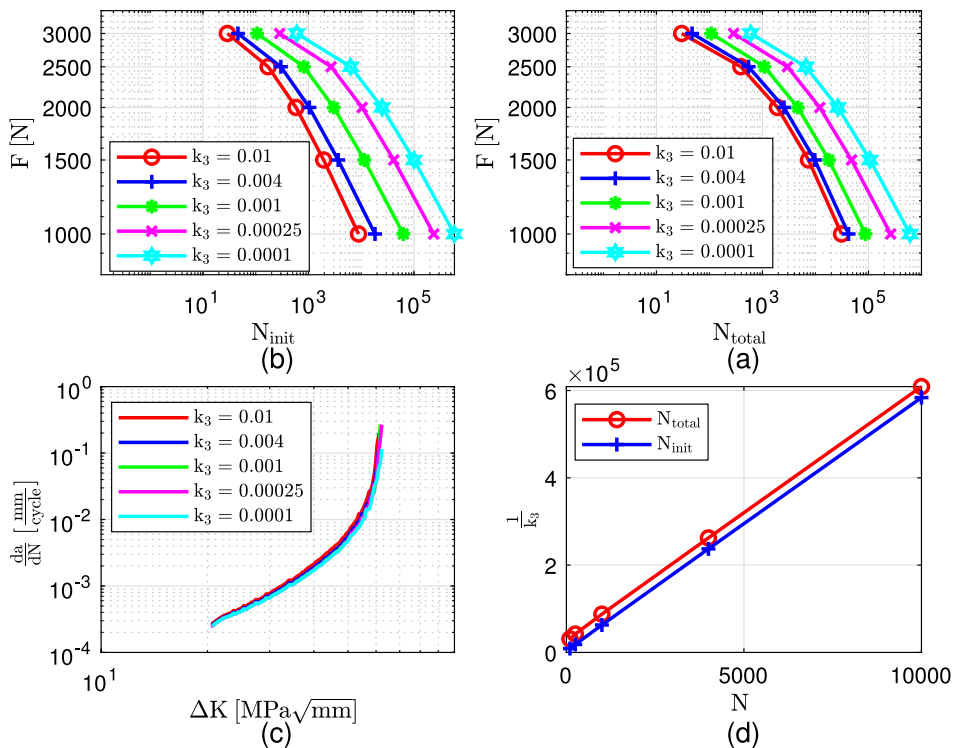


Fig. 3. Influence of k_3 parameter. Initiation $S-N$ curves (1), total life $S-N$ curves (b), Paris' curves for $F = 1000$ N (c) and cycle counts for $F = 1000$ N (d) for different values of k_3 .

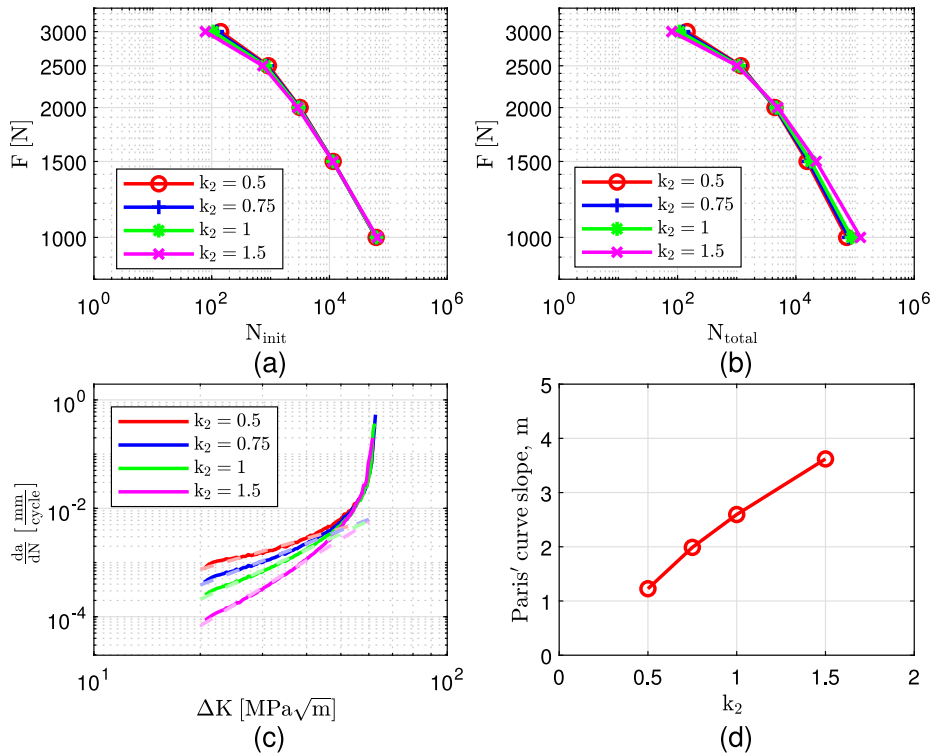


Fig. 4. Influence of k_2 parameter. Initiation $S-N$ curves (1), total life $S-N$ curves (b), Paris' curves for $F = 1000$ N (c) and calculated Paris' curve slope (d) for different values of k_2 . Paris' curve slope is calculated by fitting data from $\Delta K \approx 20$ MPa \sqrt{m} to $\Delta K \approx 40$ MPa \sqrt{m} .

value reaches some threshold value, the crack initiation driving force will always dominate crack initiation. When it comes to a crack propagation regime, it can be seen from Figs. 2 and 3 that crack propagation rate does not change significantly for wide range of values of k_1 and k_3 parameters, leading to the conclusion that the crack propagation rate is driven dominantly by the crack propagation driving force. However, the crack initiation driving force tends to change overall crack propagation rate if $k_1 < k_2$, as observed on Fig. 2c. A reason for such behaviour could be found in the fact that by lowering the k_1 parameter the accumulation rate of crack initiation driving force tends to increase for small values of $\bar{\psi}_{init}$. As the crack initiation driving force sets the lower limit for the crack growth rate, in such cases the influence of this force may become significant for very low values of k_1 . However, for most engineering metallic materials $-\frac{1}{\beta} > m$ (e.g., m for the most of metallic materials ranges from 2 to 4, while $-\beta$ ranges from 0.05 to 0.12, see. [37]), meaning that for such material $k_1 > k_2$.

From Fig. 3a and b it can be concluded that by changing the value of k_3 the $S-N$ curves are simply shifted, while Fig. 3c implies that k_3 practically does not influence crack propagation. This is further corroborated by Fig. 3d, which clearly shows that N_{init} and N_{total} change in the same way with respect to the value of k_3 . In addition, it can be seen from Fig. 3d that the number of cycles to crack initiation at a fixed load strongly follows the analytically predicted term $k_3 N = Const$. Also, the influence of k_3 on the crack propagation rate for a particular set of k_i parameters is insignificant. However, as the fatigue crack initiation driving force sets the lower bound on the crack propagation rate, it is expected that k_3 would influence the crack propagation rate only in case of extremely slow crack propagation (very small k_4). In that case, the calibration of Paris' and $S-N$ curve coefficients would be somewhat more complex, as its calibration would not be independent anymore.

As already mentioned, the influence of the fatigue crack propagation driving force is much more complex than the influence of the fatigue crack initiation driving force due to its evolution being dependent on the decoupling function F_s . As a result, performing a simplified semi-analytic analysis of the influence of model parameters k_2 and k_4 is not possible. However, the numerical results of parametric simulations are shown in Fig. 4. It can be seen that the fatigue crack propagation parameters barely influence crack initiation $S-N$ curves, shown in Fig. 4a. This can be attributed to the fact that the fatigue crack propagation driving force does not accumulate for the small values of phase-field (due to the decoupling function F_s). Further, note that a crack is considered initiated at $\phi = 0.95$. Since the fatigue crack propagation force starts to accumulate at $\phi = \phi_{thres}$, the life span from ϕ_{thres} to $\phi = 0.95$ is influenced by the crack propagation driving force. However, as the fatigue crack propagation driving force usually accumulates faster than the fatigue crack initiation driving force (due to $k_4 > k_3$), a life span from ϕ_{thres} to $\phi = 0.95$ is usually very short and does not influence the crack initiation time significantly. Consequently, the influence of the fatigue crack propagation driving force on crack initiation could be modified by changing the value of ϕ_{thres} . It is clear from Fig. 4c and d, that the Paris' curve slope (the exponent of Paris' curve) depends almost linearly on the parameter k_2 . Also from Fig. 5c and d, it can be seen that the Paris' curve

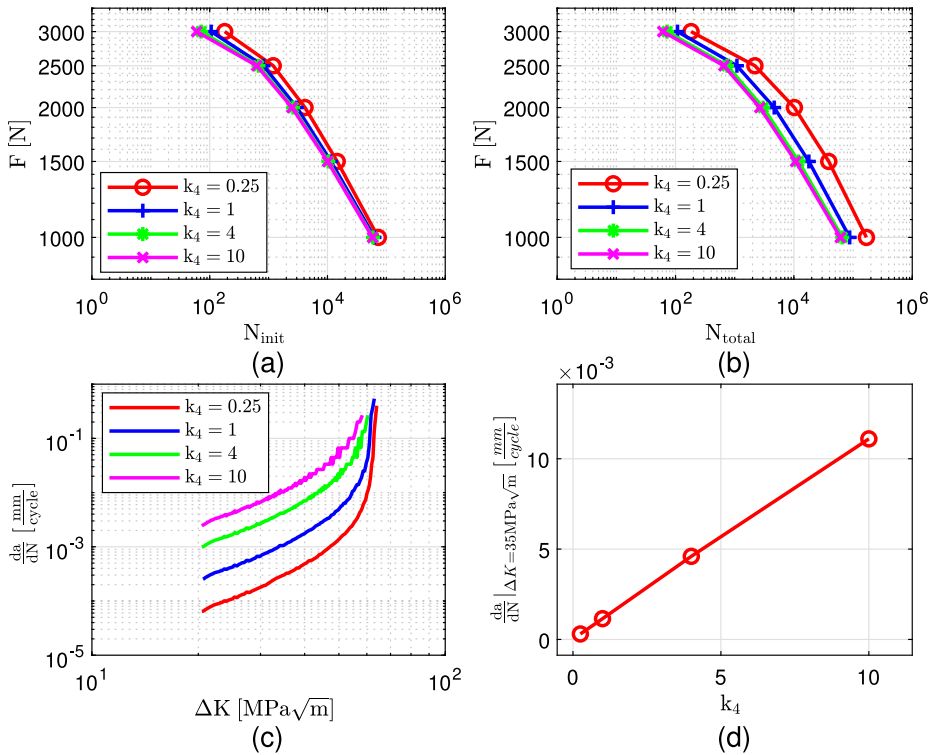


Fig. 5. Influence of k_4 parameter. Initiation $S-N$ curves (1), total life $S-N$ curves (b), Paris' curves for $F = 1000$ N (c) and calculated rates of crack growth for $K \approx 35$ $\text{MPa}\sqrt{\text{m}}$ (d) for different values of k_4 .

coefficient depends linearly on the parameter k_4 , i.e., the parameter k_4 scales the crack growth rate linearly. However, since the lower bound of the crack growth rate is set by the fatigue initiation driving force, this might not be valid any more if the fatigue crack initiation driving force is dominant over the fatigue crack propagation driving force.

The influence of ϕ_{thres} is investigated next and the results, obtained for all other parameters fixed at their default values (see Section 4.1), are shown in Fig. 6. It can be seen that ϕ_{thres} delays crack initiation slightly, and reduces the crack propagation rate more significantly. This is both expected because higher ϕ_{thres} delays the accumulation of the fatigue crack propagation driving force, but also reduces the region where the fatigue crack propagation driving force can be accumulated. Consequently, it is expected that higher ϕ_{thres} would lead to less phase-field smearing due to a smaller width of the zone where the fatigue crack propagation driving force achieves high values.

Further, the influence of G_c and l is examined, while holding all other parameters fixed. Default parameters given in Section 4.1 are used, with $G_{c,0} = 35.31$ MPa mm and $l_0 = 0.4582$ mm . From 7a and b it can be observed that the increase in G_c increases the fatigue life for constant applied forces. By recalling fact that $F \propto \sqrt{\psi}$ and $F_{\text{crit}} \propto \sqrt{G_c} \propto \sqrt{\psi_{\text{crit}}}$, and by noticing that the accumulation of the crack driving forces is proportional to $\psi_{\text{crit}}(\psi_0^+/\psi_{\text{crit}})^{k_1}$ and $\psi_{\text{crit}}(\psi_0^+/\psi_{\text{crit}})^{k_2}$ and that the accumulated fatigue driving forces that lead to the failure are proportional to ψ_{crit} , it could be deduced that the applied forces F that lead to the equal number of cycles to failure are proportional to F_{crit} . This is clearly depicted in Fig. 7b, where the plot $\frac{F}{F_{\text{crit}}} - N$ is insensitive to G_c . Note that the proportionality of critical forces and critical energy release rates can be attributed to proportionality/similarity of displacement fields, which can be derived by means of dimensional analysis.

The same does not hold for the influence of the length-scale parameter, which is visible in Fig. 7c and d. Here the plots $\frac{F}{F_{\text{crit}}} - N$ obtained for different l are not completely overlapping, because a change in l modifies not only the value of σ_{crit} , but also leads to dissimilar distributions of displacement and strain fields. Additionally, the loss of overlap can be attributed to the fact that, unlike the change of σ_{crit} , the change of F_{crit} is usually not proportional to $\frac{1}{\sqrt{l}}$.

The results presented in this chapter suggest that the proposed model could be relatively easily calibrated from experimentally obtained $S-N$ and Paris' curves. To facilitate the calibration procedure, the following observations should be taken into account:

- The parameters k_2 and k_4 have minimal influence on the initiation $S-N$ curves. Consequently, if available, these curves could be used to identify the parameters k_1 and k_3 , defining the crack initiation driving force. Alternatively, the fact that the parameters k_1 and k_3 do not have a significant influence on the Paris' crack growth curve if $k_1 > k_2$ and $k_3 \ll k_4$ can be exploited. In that case first the Paris' curve could be used to identify the parameters k_2 and k_4 , whereupon the parameters k_1 and k_3 could be characterised from the total life $S-N$ curve (the life up to complete failure).

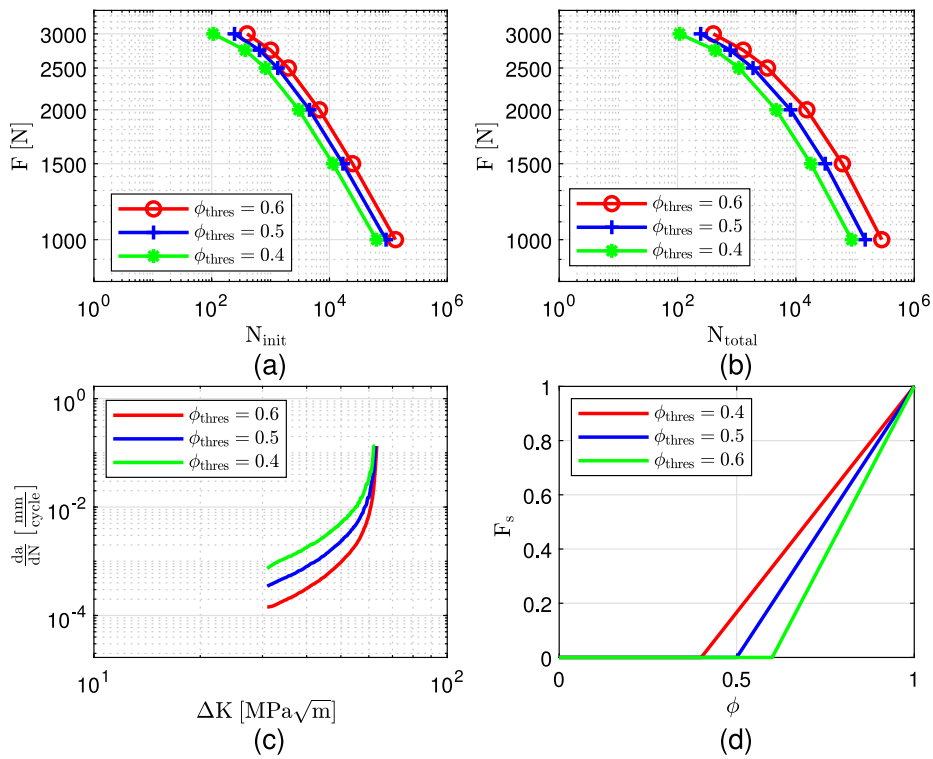


Fig. 6. Influence of ϕ_{thres} parameter. Total life $S-N$ curves (1), initiation $S-N$ curves (b), Paris' curves for $F = 1500$ N case (c) and decoupling functions F_s (d) for different values of ϕ_{thres} .

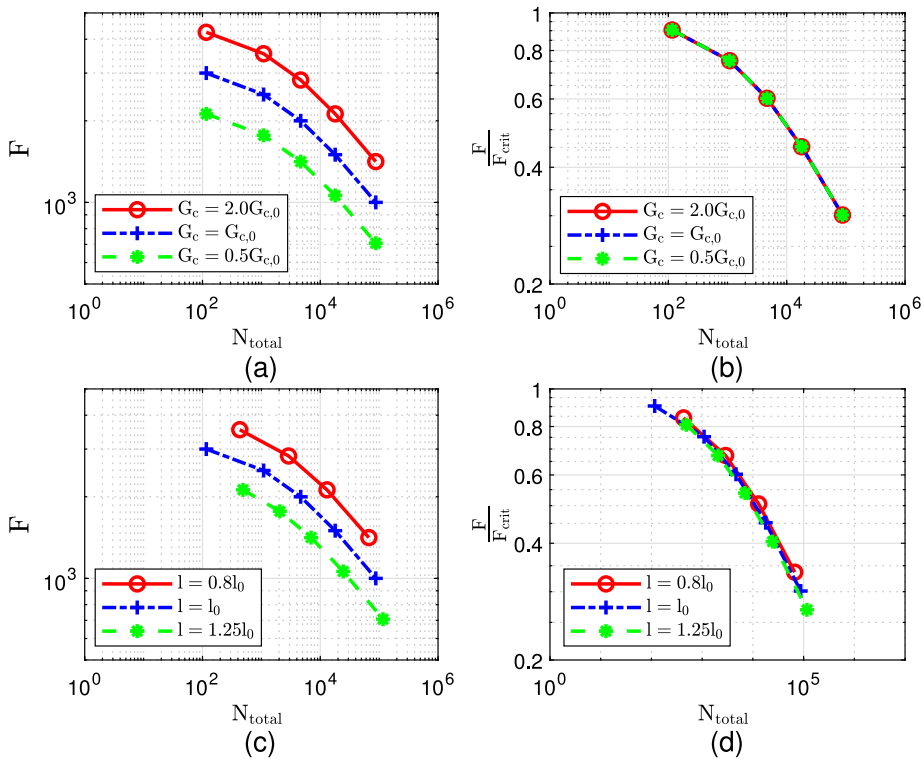


Fig. 7. $\frac{F}{F_{crit}} - N$ plots: for different G_c (a–b), for different l (c–d).

- The model response could be further tuned up by choosing appropriate values of parameters ϕ_{thres} (or by choosing a coupling function F_s different from Eq. (15)) and f in Eqs. (9)–(10). In general, ϕ_{thres} controls the activation of the crack propagation driving force, while f controls the localisation of damage and the accumulation rate of fatigue crack driving forces.

From the above considerations, it could be concluded that the proposed model could enable better simultaneous reproduction and prediction of S - N curves and crack growth curves in comparison to the majority of PF fatigue models containing only 1 or 2 fatigue parameters, which typically depend on at least two classical fatigue parameters. This coupling of classical parameters might severely hamper accurate reproduction of fatigue phenomena by such models.

4.3. Mean stress effect

In this subsection, the effect of mean stress is considered. It should be emphasised that, since the fatigue driving forces are based on ψ_0^+ , compressive stress states should not affect fatigue life. Therefore, only pure tensile cases are considered. For the purpose of preliminary analysis, the following quantities are introduced,

$$F_{\text{mean}} = \frac{F_{\text{max}} + F_{\text{min}}}{2}, F_a = \frac{F_{\text{max}} - F_{\text{min}}}{2}, F_r = F_{\text{max}} - F_{\text{min}}, R = \frac{F_{\text{min}}}{F_{\text{max}}}, \quad (66)$$

where F_{mean} stands for the mean force, F_a is the force amplitude, F_r is the force range, F_{max} and F_{min} are the maximal and the minimal force, respectively, and R denotes the load ratio.

Now, we again consider crack initiation for simple homogeneous stress and phase-field distributions with a constant loading cycle. As before, the fatigue crack propagation driving force is neglected for simplicity. Nevertheless, as suggested by the presented results, the following analysis is still valid for all cases with the crack initiation time much larger than the crack propagation time. Starting from the expression (9), it can be assumed that the accumulation of fatigue initiation driving force in one cycle is proportional to $k_3 \left(\sigma_{\text{max}}^{2k_1} - \sigma_{\text{min}}^{2k_1} \right)$. Further assuming that σ is proportional to F , the accumulation of fatigue crack initiation driving force during one cycle is now

$$\psi_{\text{init},1} \propto k_3 \left((F_{\text{max}})^{2k_1} - (F_{\text{min}})^{2k_1} \right). \quad (67)$$

Next, we introduce a force that leads to the same damage for $R = 0$, denoted here as F_{eqv} . Since $F_{\text{min}}(R = 0) = 0$, it means that $F_{\text{eqv}} = F_{\text{max}}(R = 0)$ should induce the fatigue initiation crack driving force identical to the one caused by the real load, defined by Eq. (67), leading to:

$$F_{\text{eqv}} = \left((F_{\text{max}})^{2k_1} - (F_{\text{min}})^{2k_1} \right)^{\frac{1}{2k_1}}. \quad (68)$$

Norming it in terms of F_{max} , it can be written as:

$$F_{\text{eqv}} = F_{\text{max}} \left(1 - (R)^{2k_1} \right)^{\frac{1}{2k_1}}. \quad (69)$$

Alternatively, using $F_r = F_{\text{max}}(1 - R)$ and $F_{\text{mean}} = \frac{F_{\text{max}}}{2}(1 + R)$, F_{eqv} could be alternatively expressed in terms of F_r and F_{mean} . Using the fact that according to Eq. (66) $F_{\text{max}} = F_{\text{mean}} + \frac{F_r}{2}$ and $F_{\text{min}} = F_{\text{mean}} - \frac{F_r}{2}$ Eq. (67) can be rewritten as a family of Haigh's curves:

$$\psi_{\text{init},1} \propto \left(F_{\text{mean}} + \frac{1}{2} F_r \right)^{2k_1} - \left(F_{\text{mean}} - \frac{1}{2} F_r \right)^{2k_1} = \frac{\text{Const}}{k_3}. \quad (70)$$

In general, it is not possible to find an explicit dependence of F_r on F_{mean} from a Haigh curve. However, one can analyse simple cases with $k_1 = 0.5$ and $k_1 = 1$ for a known k_3 . By inserting $k_1 = 0.5$ into (70), one obtains $F_r = \text{Const}$, implying that there would not be any mean stress effect. In case of $k_1 = 1$, Eq. (70) delivers term $F_{\text{mean}} F_r = \text{Const}$, which is the only Haigh's curve with an explicit dependence of F_{mean} and F_r . In addition, it can be seen that k_3 does not influence the shape of a Haigh's curve, but rather scales it by simultaneously changing F_{mean} and F_r necessary to guarantee a requested initiation, i.e., the total life. It can be concluded that by ignoring the fatigue crack propagation driving force, the mean stress effect could be efficiently controlled by k_1 , as visible from Fig. 8b, since this parameter governs the shape of Haigh's curves. From Eqs. (69)–(70) and Fig. 8a it follows that $k_1 = 1/2$ leads to $F_{\text{eqv}} = F_{\text{max}}(1 - R) = F_r$, i.e., there is no mean stress effect, while by increasing k_1 , the value of F_{eqv} tends toward the value of F_{max} , implying a more pronounced mean stress effect.

Fig. 8b shows different possible shapes of Haigh's curves. If the crack propagation time takes a significant part of the total life, and the fatigue crack propagation driving force is included, the mean stress phenomenon is much more complex to analyse. In that case, a numerical parametric study is necessary to identify the effect of each parameter on the mean stress effect, which is outside the scope of this paper.

In the following, the potential of the proposed model to capture the mean stress is demonstrated for the cases when the crack initiation time is significantly larger than the crack propagation time. Note that this is typical for relatively smooth notched structural components subjected to relatively low stresses (see e.g. [38] and references therein). The crack initiation time can sometimes be dominant in the HCF regime, and is crucial in the Ultra-High Cycle Fatigue (UHCF) of commercial materials. (see e.g. [39]). Such scenarios can be described by the proposed model if the fatigue parameter values are set up so that $k_4 > k_3$ (see Section 4.2). As explained by the previous analytical analysis, it is expected that in this case the parameter k_1 is to play a dominant role in describing the mean stress effect. The results of the study are presented in Fig. 9, obtained by setting up $k_1 = 2$, $k_2 = 1$, $k_3 = 0.001$ and $k_4 = 1$.

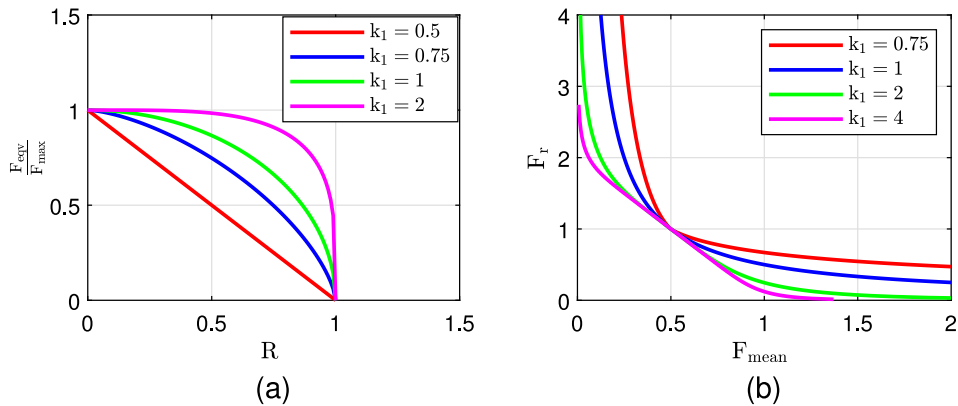


Fig. 8. Plot of (69) (a) and Haigh's curves predicted by (70) (b) for different values of k_1 .

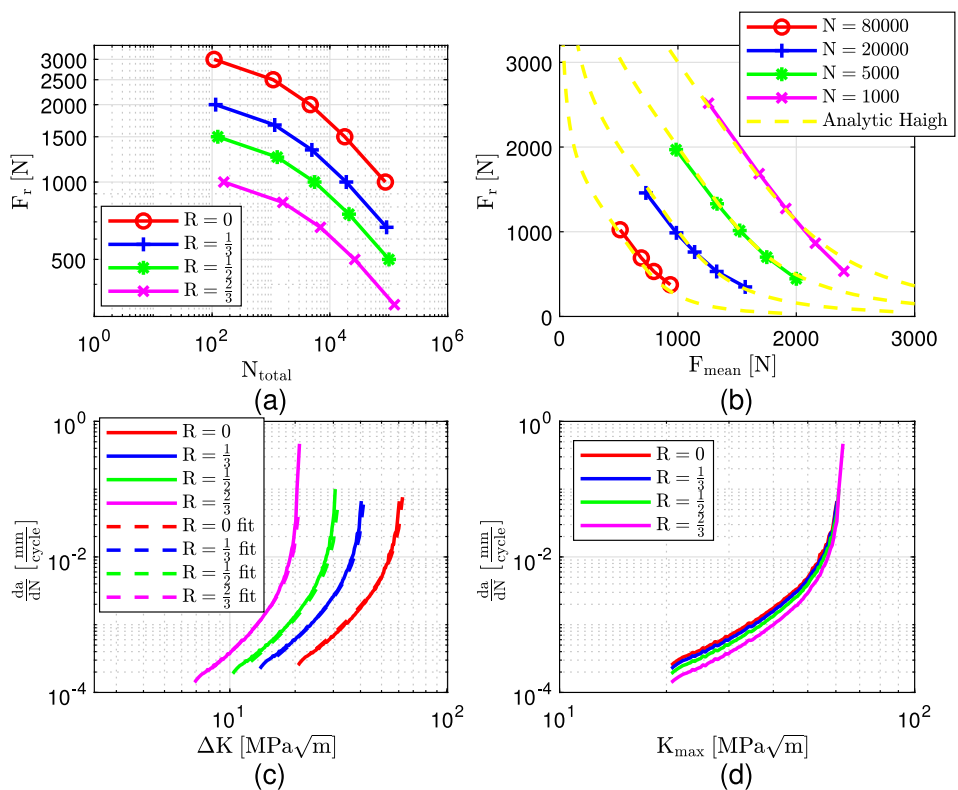


Fig. 9. Influence of mean stress. Total life $S-N$ curves (1), Haigh's curves (b), Paris' curves for $F = 1000$ N, numerically obtained and approximation by Eq. (71) (c) and $\frac{da}{dN} - K_{max}$ curves for $F = 1000$ N (d) for different values of R .

The load ratio R is varied so that for each R the maximal forces $F_{max} = \{3000, 2500, 2000, 1500, 1000\}$ are used. The total life $S-N$ curve (the life up to complete failure) for various R , with F_r on the ordinate, are depicted in Fig. 9a, and the influence of the mean stress is clearly visible. However, it can be observed from Eq. (69) and Fig. 8a that for $k_1 = 2$ and the considered values of R the statement $F_{eqv} \approx F_{max}$ is valid. This implies that the obtained numerical results are consistent with the previous observation, obtained by completely ignoring crack propagation, that for relatively large k_1 the model should demonstrate the sensitivity towards the mean stress effect. Additionally, the numerically obtained Haigh diagrams shown in Fig. 9b do agree well with the analytical curves defined by the right-hand side of Eq. (70), once more confirming the validity of previous theoretical predictions. Interestingly, the obtained Haigh's curves are convex, same as the Smith's curve, that is according to [40] representative for brittle materials.

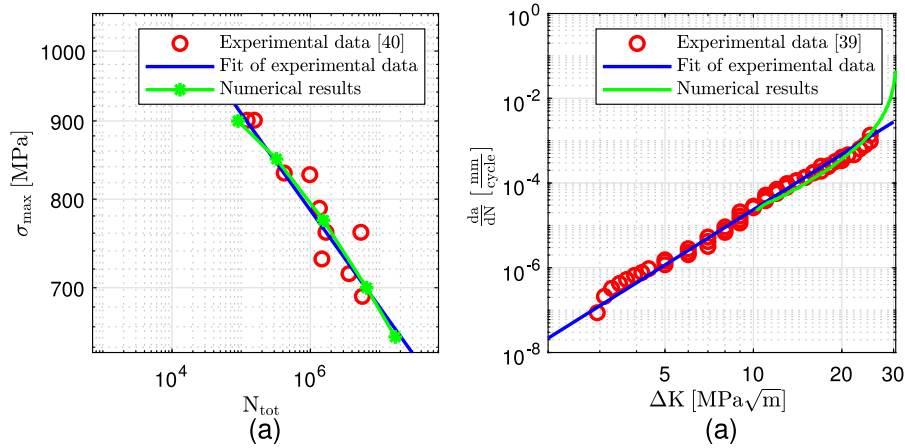


Fig. 10. Stress-life data from experiment [44] and numerical simulations (a) and Paris' curves from experiment [43] and numerical simulations (b).

Additionally, it can be shown that the influence of R on the crack growth rate for the results shown in Fig. 9c could be fitted well with equation:

$$\frac{da}{dN} = C \left(\frac{\Delta K}{(1-R)^{1-\bar{\gamma}}} \right)^n \frac{1}{1 - \frac{K_{\max}}{K_c}}, \quad (71)$$

where $C \left(\frac{\Delta K}{(1-R)^{1-\bar{\gamma}}} \right)^n$ is the term in Walker's equation [41], while $\frac{1}{1 - \frac{K_{\max}}{K_c}}$ is borrowed from NASGRO equation [42] to obtain an accurate fit in final stages of crack growth. The parameters used for the fit are $C = 3.5 \cdot 10^{-7} \frac{\text{mm}}{\text{cycle} \cdot (\text{MPa}\sqrt{\text{m}})^n}$, $n = 2.066$, $\bar{\gamma} = 0.3$ and $K_c = 64 \text{ MPa}\sqrt{\text{m}}$.

4.4. Calibration example

In this subsection, a characterisation of the fatigue model parameters is performed on titanium Ti-6Al-4V. As it is extremely hard to find complete data, for this demonstrative example the material parameters and fatigue data are combined from multiple papers. Although material parameters can vary from batch to batch and combining data could be inappropriate in solving practical problems, here this is done only for the purpose of demonstration of calibration capabilities of the proposed model. A more precise calibration from the experimental data obtained in a systematic manner should be ideally performed and will be the subject of future work on the matter. In addition, here plasticity is neglected and the material is assumed to be brittle.

Material parameters are defined as follows: the Young modulus is $E = 116000 \text{ MPa}$ (from [43]), the Poisson ratio is $\nu = 0.33$, $K_c = 64 \text{ MPa}\sqrt{\text{m}}$ (data in the available literature range from $50 \text{ MPa}\sqrt{\text{m}}$ to $100 \text{ MPa}\sqrt{\text{m}}$), i.e., $G_c = 35.31 \text{ MPa mm}$ and the critical stress is $\sigma_{\text{crit}} = 970 \text{ MPa}$ (from [43]). Experimental stress-life data (taken from [44]) for $R = 0.5$ is shown in Fig. 10a and the experimental Paris' curve (taken from [43]) for the $R = 0.5$ case is shown in Fig. 10b. Although some other models would be more suitable, for sake of simplicity the AT2 model is used, leading to $l = 0.4582 \text{ mm}$. The numerically calculated Paris' curve shown in Fig. 10b was calculated on CT specimen with $\Delta F = 500 \text{ N}$, while the smooth rounded bar was simplified to 1-D bar with a length of 20 mm and discretised with 200 elements. In the case of the CT specimen, a force range lower than 500 was not considered for the sake of computational costs. During the simulation of the smooth rounded bar, the tensile part of energy density was assumed to be the total energy density (as in the isotropic energy split), because critical stress (i.e., length-scale parameter) was derived with such assumption. The k_i parameters were fitted, while $\phi_{\text{thres}} = 0.4$ and $f = 1$ were assumed.

The results obtained after calibration are shown in Fig. 10. A good fit of both the $S-N$ and Paris' curve has been obtained with parameters $k_1 = 5$, $k_2 = 1.6$, $k_3 = 0.000135$ and $k_4 = 0.4$. This confirms that the proposed model is suitable for the calibration of (high-cyclic) fatigue behaviour of realistic materials.

4.5. Other observations

In this subsection, some secondary features of model that are not directly related to fatigue behaviour are addressed. This includes both advantageous and disadvantageous features.

4.5.1. Geometry dependence

It is demonstrated that the fatigue crack growth rate is not influenced by geometry. The Paris' curve for the CT and TPB specimens are compared and the obtained results are shown in Fig. 11. As visible from the curves, equal crack growth rates have been obtained for all considered setups, leading to the conclusion that the model is not geometry dependent.

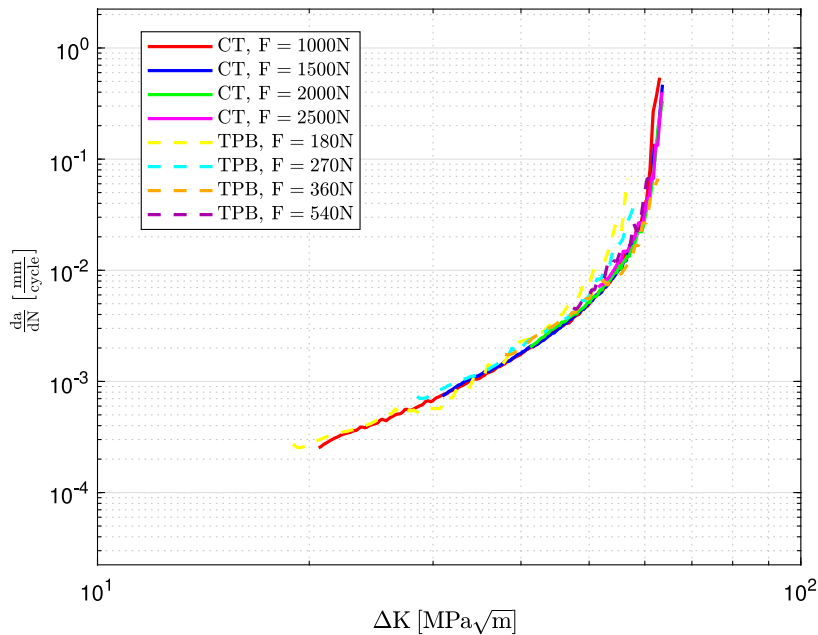


Fig. 11. Obtained Paris' curves for CT and TPB specimens with same fatigue parameters.

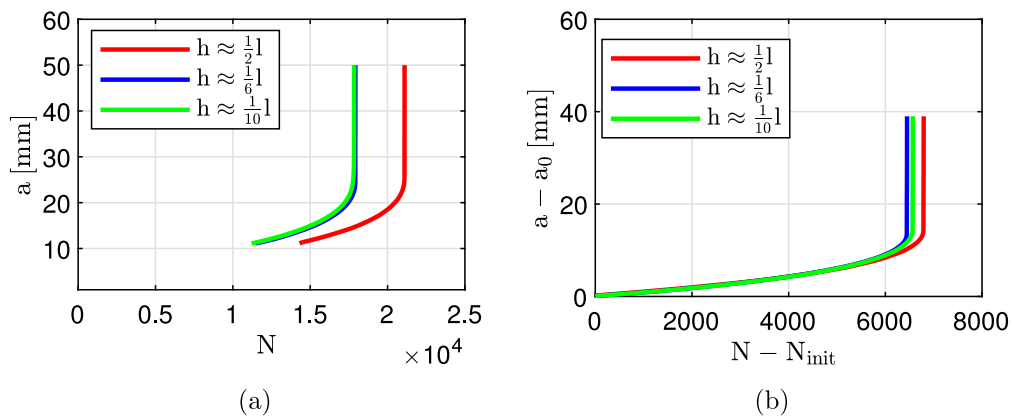


Fig. 12. Mesh sensitivity, total life including initiation and propagation cycles (a), crack propagation cycles (b).

4.5.2. Mesh influence

The influence of mesh size is studied next. The CT specimen was considered with forces $F_{\max} = 1500$ N and $F_{\min} = 0$ N. Different meshes with the element sizes $\frac{h}{l} = \left\{ \frac{1}{2}, \frac{1}{6}, \frac{1}{10} \right\}$ were applied in the region where the crack propagation was expected. Here, h denotes the edge length of elements in the refined zone. From the results presented in Fig. 12, it can be seen that, although a small difference exist between the results obtained with $h = \frac{1}{6}$ and $h = \frac{1}{10}$, a convergence tendency can be observed, and the results for $h = \frac{1}{6}$ are considered valid. Therefore, since computation costs are much smaller for $h = \frac{1}{6}$, the meshes with $h = \frac{1}{6}$ in the regions where fracturing is expected are used in all other simulations. Also, one can see from Fig. 12 that the mesh $h = \frac{1}{2}$ produces a considerably different prediction of the crack initiation life than denser meshes, while difference in the total propagation cycles is much smaller. This is probably due to the fact that the mesh $h = \frac{1}{2}$ is not sufficiently dense to resolve the displacement field correctly around the notch on CT specimen, leading to smaller stresses and strains, and consequently a slower rate of the growth of the fatigue crack initiation driving force. In addition, $h = \frac{1}{2}$ mesh is insufficient to resolve phase-field profile properly in case of monotonic loading failure, leading to overestimation of fracture energy, and therefore it is expectable that such mesh will also lead to wrong fatigue life predictions.

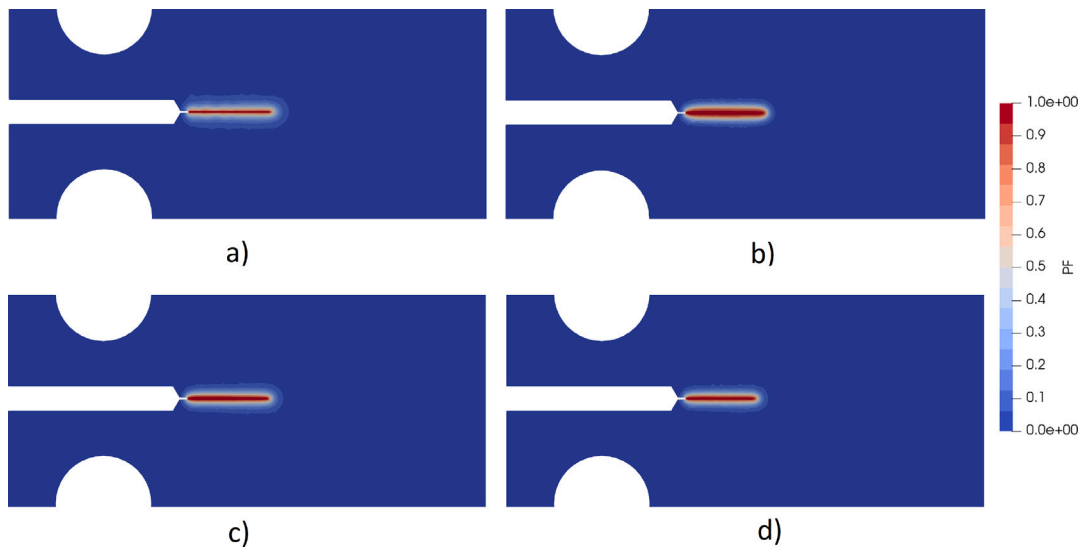


Fig. 13. Phase-field profile obtained for monotonic loading (a), for fatigue case with $k_2 = 1$ and $\phi_{\text{thres}} = 0.4$ (b), for fatigue case with $k_2 = 1$ and $\phi_{\text{thres}} = 0.6$ (c) and for fatigue case with $k_2 = 1.5$ and $\phi_{\text{thres}} = 0.4$ (d). In all cases the value of length-scale is $l = 0.4582$ mm. For compactness, the section of CT specimen's geometry is shown.

4.5.3. Phase-field profile widening

In Fig. 13, the phenomenon of phase-field profile widening during fatigue fracture is illustrated. It can be observed that during the stable phase of fatigue crack growth the phase-field profile widens, resulting in a profile that is very different from the analytical one (and one that is characteristic to unstable propagation). Obviously, the phase-field profile widens due to the fact that the fatigue crack driving forces slowly accumulate through whole domain, leading to a smeared distribution of fatigue crack driving forces, while during brutal crack propagation crack driving force is localised in a thin band. The extent of such widening is influenced by ϕ_{thres} , f and k_2 parameters, and each is discussed in following paragraphs.

By comparing Fig. 13b and d, it can be shown that the extent of the phase-field profile widening depends on the k_2 parameter. It can also be argued that it also depends on k_1 , but it is harder to quantify its influence, since the fatigue crack propagation driving forces are usually dominant during crack propagation. For the smaller values of parameters, the widening is larger. This can be easily explained, since for strain energy densities that are smaller than the critical value, the accumulation rates of fatigue crack driving forces will be higher as k_1 and k_2 decrease, leading to higher crack driving forces in zones with small strain energy density. The smallest recommended k_1 and k_2 are around 0.75, and by authors experience, anything less than 0.75 will lead to excessive widening.

The phase-field widening can be reduced by increasing ϕ_{thres} , since that enforces a narrower area capable of producing the fatigue propagation driving force. Some small reduction can be seen by comparing Fig. 13b and c, where ϕ_{thres} was increased from 0.4 to 0.6.

Another parameter that affects the widening of phase-field profile is f . To analyse it, we consider how the fatigue crack driving forces accumulate in the limit cases when $f = 0$ and $f = 2$, in a simple 1-D homogeneous setup. In case of $f = 0$ (from Eqs. (9) and (10)) it is obvious that the undegraded tensile strain energy density drives the accumulation of crack driving forces. As the strain energy is usually higher in damaged zones, the accumulation rate of fatigue crack driving forces will also be higher, leading to the increased localisation of the phase-field distribution. However, for $f = 2$, the accumulation rate of crack driving forces will be proportional to the square of degraded tensile stress. As in the considered 1-D setting the stress distribution is constant, it can be concluded that the accumulation of crack driving forces will tend to be uniform for $f = 2$, leading to phase-field distribution with highest extent of smearing.

4.5.4. Monotonic loading

It is shown here that the proposed model is also suitable for monotonic loading. In Fig. 14 the influence of the fatigue parameters is shown for the monotonically loaded CT specimen, with $k_1 = 2$ and $k_2 = 1$. It can be seen that a very small change in the critical force (by order of magnitude of 0.1%) is obtained for the wide range of k_3 and k_4 parameters. However, very high values of k_3 and k_4 would drastically change monotonic loading behaviour. Theoretically, this effect could be quantified for some simple 1-D cases.

For simplicity, assume a special 1-D case with homogeneous stress and phase field distributions, caused by monotonic loading, with $k_1 = 1$, $k_4 = 0$ and arbitrary k_3 . Now, for $f = 0$ the phase-field evolution equations can be rewritten as:

$$\frac{dg}{d\phi} \psi_0^+ (1 + k_3) + \frac{\partial \gamma}{\partial \phi} G_c = 0. \quad (72)$$

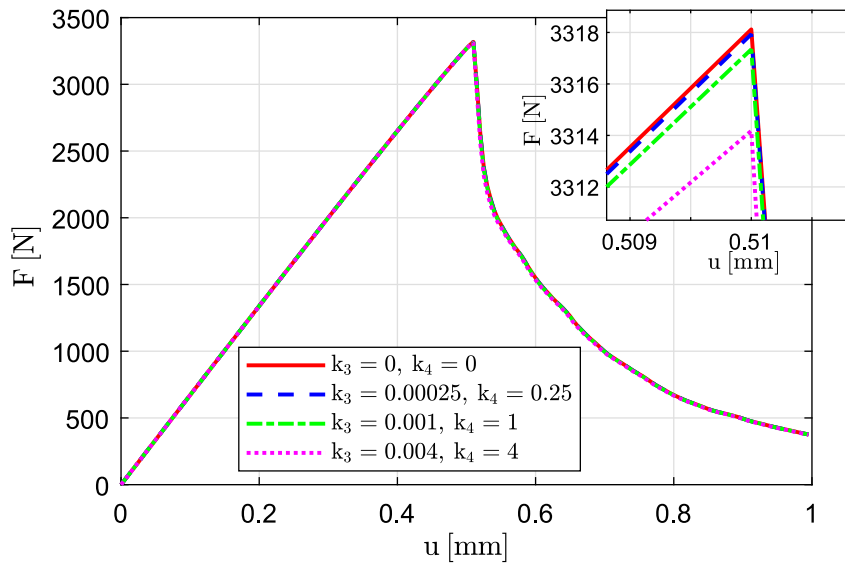


Fig. 14. Influence of fatigue parameters on response under monotonic loading.

It is clear that for this special case the introduction of fatigue crack initiation driving force increases the total crack driving force by factor of $1 + k_3$ and accordingly reduces the critical stress and strain, as well as the critical deformation energy.

The parameter f can also influence monotonic behaviour. For example, for $f = 2$ accumulation of fatigue crack driving force stops at peak the stress, while for $f = 0$ accumulation continues through whole loading process, leading to a conclusion that a lower f exhibits a higher influence on behaviour during monotonic loading.

When it comes to the influence of fatigue crack propagation force, it is much harder to quantify it, as it depends on the decoupling function F_3 (see Eqs. (9) and (10)). It should be noticed that if the threshold value of phase-field ϕ_{thres} is higher than the critical value of phase-field in monotonic loading ϕ_{crit} (the value of phase-field at the peak stress for homogeneous 1-D case), then the fatigue crack propagation driving force will not influence pre-critical behaviour even for the high value of k_4 . However this assumption is limited to simple 1-D cases with the homogeneous distributions of phase-field and stress. From Fig. 14 it can be seen that the load–displacement curve for the considered example is not influenced significantly even by high values of k_4 . If the influence of the fatigue crack driving force on monotonic loading is too high, the approach of [23] can be used, where the evolution of fatigue history variable additionally depends on a (standard) history variable in a way that prevents fatigue crack driving forces do not accumulate during monotonic loading.

4.5.5. Complex case and influence of energy split

Further, a problem involving multiple cracks is analysed. The goal is to show that the proposed model is capable of reproducing meaningful crack patterns even for complex geometry. In addition, the definition of the degrading strain energy is shortly discussed. The model should be able to yield a complex crack patterns with cracks aligned with the load direction for compressive cases and crack patterns with cracks aligned with the direction perpendicular to the applied load for tensile cases. A plate with 17 holes with random distribution and size is considered. The geometry and boundary conditions from Fig. 15a are adopted. Tensile loading with the load ratio $R = 0$ with $u_{\text{max}} = 0.1$ mm and compressive loading with the load ratio $R = -\infty$ with $u_{\text{min}} = -0.36$ mm are imposed. The used material parameters are $k_1 = 2$, $k_1 = 1$, $k_3 = 0.02$, $k_4 = 1$ and $l = 0.2$ mm. Here two models are used:

- the anisotropic model, with the Freddi's split used for both the stresses and crack driving forces,
- the hybrid model, where the isotropic degradation (the degradation of entire deformation energy) is used for the stress calculation, and the Freddi's energy split is applied for the definition of crack driving forces.

In Fig. 16, it can be seen that, as hypothesised, we obtain cracks dominantly oriented in the direction of the applied load for compressive cases, and cracks dominantly oriented perpendicularly to the applied load in case of tensile loading, thus confirming that the proposed model can handle complex geometries and crack patterns.

Motivation for introducing the hybrid model can be seen in Fig. 16a and b. It can be seen that the results for the anisotropic model (Fig. 16a and b) lead to a considerable widening of the phase-field profile. On the other hand, this issue is less pronounced in case of the hybrid model. It could be assumed that this phase-field widening in the anisotropic model is caused by the shear transmission, induced by the applied spectral split. This is a common deficiency of the spectral energy splits, and can be alleviated by applying directional splits. However, this is still an open topic of active research and only few papers are available on that

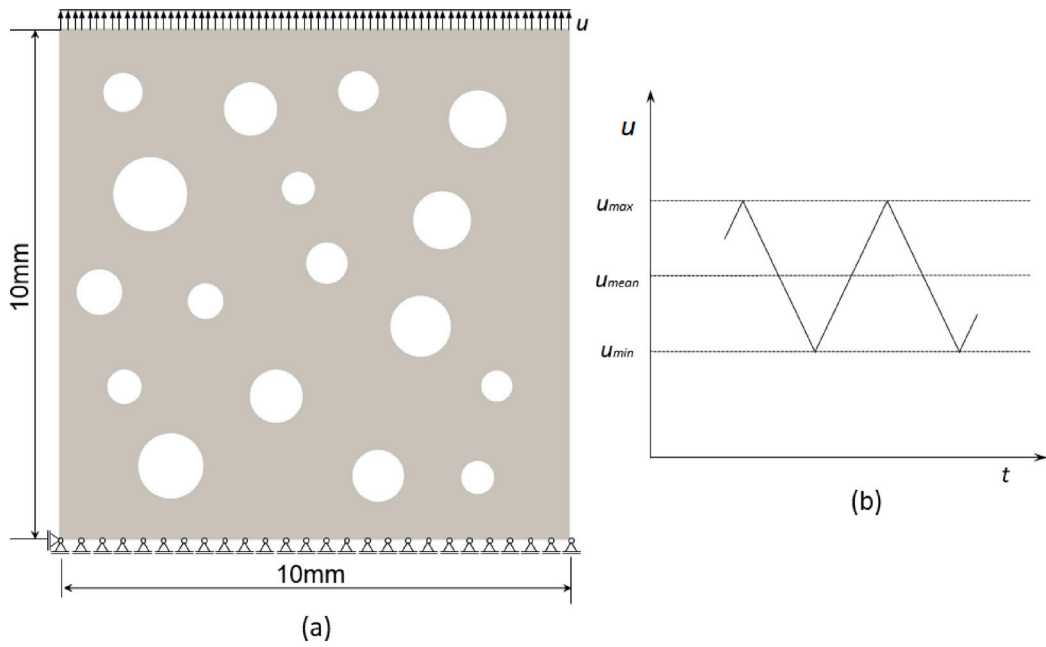


Fig. 15. Geometry (a) and load cycle (b).

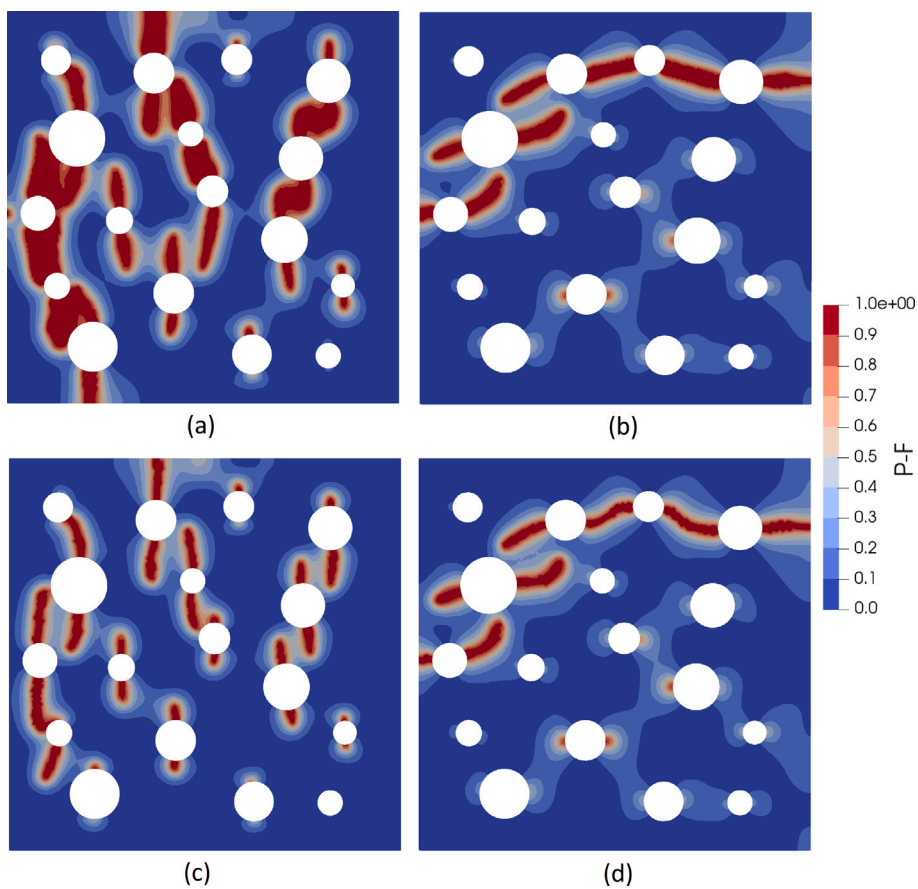


Fig. 16. Plate with multiple holes: anisotropic model for $R = -\infty$ after 1500 loading cycles (a), anisotropic model for $R = 0$ after 3000 loading cycles (b), hybrid model for $R = -\infty$ after 1500 loading cycles (c), hybrid model for $R = 0$ after 3000 loading cycles (d).

subject (including [45–48]). Alternatively, splits with the degradation of deviatoric strain energy could also be used. However, further research and discussion is out of scope of this paper.

5. Conclusion

In this work a new multi-parameter PF model for fatigue fracture is presented, based on the concept of adding new crack driving forces accounting for fatigue phenomena. In this work, only the high-cyclic fatigue has been considered, and the standard AT2 model for brittle fracture have been extended to deal with fatigue. The influence of each model fatigue parameter is explored and analysed in detail, focusing on the ability of the model to describe $S-N$ and Paris' curves. In addition, the obtained crack patterns are inspected, to reveal more aspects of the model. The main advantage of the proposed model is the potential of the model to be calibrated from experimental data to reproduce accurately both the $S-N$ curve or the Paris law. This is due to the fact that the model is equipped with 2 pairs of parameters, which are to a large degree mutually independent and describe well either the $S-N$ curve or the Paris law. In addition, each of the model parameters dominantly influences only one classical material fatigue parameter in an almost linear fashion, potentially enabling relatively easy calibration of the model. Certain restrictions which might affect the calibration process, have been identified, like the influence of the fatigue initiation crack driving force on crack propagation, which sets the lower bound on the rate crack propagation in some cases.

In addition, the model exhibits some other desirable characteristics. For reasonably small values of the Paris' and the $S-N$ curve coefficients, the fatigue extension (additional dissipation term) practically does not influence the behaviour of the PF model under monotonic loading. Furthermore, the results suggest that the proposed model correctly predicts the Paris' curves independently of geometry.

The model is able to capture complex fatigue crack patterns, but in some cases unnatural widening of the PF profile induced by cyclic loading can be observed. It seems that this widening is significantly influenced by the choice of parameters k_2 , f and ϕ_{thres} . However, this unwanted phenomenon could also be significantly dependent on the choice of the energy decomposition, and this hypothesis should be explored in more detail in further research.

The future lines of research will be dedicated to the more detailed experimental calibration of the presented model. Other existing issues should also be considered, like fully controlling the mean stress effect, explicitly modelling other fatigue features like the endurance limit and the crack growth threshold, or addressing problem of artificial widening of PF profile. A successful solution of these problems could lead to a fully calibratable PF model for fatigue fracture, ready to be implemented for modelling realistic engineering materials.

CRedit authorship contribution statement

K. Jukić: Writing – original draft, Software, Methodology, Investigation, Conceptualization. **M. Ambati:** Writing – review & editing, Software, Methodology, Investigation, Conceptualization. **T. Jarak:** Writing – review & editing, Writing – original draft, Supervision, Conceptualization. **M. Kästner:** Writing – review & editing. **Z. Tonković:** Writing – review & editing, Project administration, Funding acquisition.

Declaration of competing interest

The authors declare that they have no known competing financial interests or personal relationships that could have appeared to influence the work reported in this paper.

Data availability

Data will be made available on request.

Acknowledgements

This work has been supported by the European Union through the European Regional Development Fund, Operational Programme “Competitiveness and Cohesion” 2014–2020 of the Republic of Croatia, project “Protection of Structural Integrity in Energy and Transport” (Zacjel, KK.01.1.1.04.0056).

References

- [1] Wöhler Alfred. Über die festigkeitsversuche mit eisen und stahl. Ernst & Korn; 1870.
- [2] Paris Paul, Gomez MP, Anderson WE. A rational analytic theory of fatigue. *Trend Eng* 1961;13(4):9–14.
- [3] Griffith AA. The phenomena of rupture and flow in solids. *Philos Trans R Soc Lond Ser A Math Phys Eng Sci* 1921;221:163–98.
- [4] Irwin George R. Fracture dynamics. *Fract Met Am Soc Met* 1948;147–66.
- [5] Irwin George Rankin. Onset of fast crack propagation in high strength steel and aluminum alloys. Technical report, Naval Research Lab Washington DC; 1956.
- [6] Sukumar N, Dolbow JE, Moës Nicolas. Extended finite element method in computational fracture mechanics: a retrospective examination. *Int J Fract* 2015;196(1):189–206.
- [7] Francfort GA, Marigo Jean Jacques. Revisiting brittle fracture as an energy minimization problem. *J Mech Phys Solids* 1998;46(8):1319–42.

- [8] Ambrosio Luigi, Tortorelli Vincenzo Maria. Approximation of functional depending on jumps by elliptic functional via t-convergence. *Comm Pure Appl Math* 1990;43(8):999–1036.
- [9] Mumford David Bryant, Shah Jayant. Optimal approximations by piecewise smooth functions and associated variational problems. *Comm Pure Appl Math* 1989.
- [10] Bourdin Blaise, Francfort GA, Marigo Jean Jacques. Numerical experiments in revisited brittle fracture. *J Mech Phys Solids* 2000;48(4):797–826.
- [11] Caputo Michele, Fabrizio Mauro. Damage and fatigue described by a fractional derivative model. *J Comput Phys* 2015;293:400–8.
- [12] Amendola G, Fabrizio M, Golden JM. Thermomechanics of damage and fatigue by a phase field model. *J Therm Stresses* 2016;39(5):487–99.
- [13] Boldrini JL, Barros de Moraes EA, Chiarelli LR, Fumes FG, Bittencourt ML. A non-isothermal thermodynamically consistent phase field framework for structural damage and fatigue. *Comput Methods Appl Mech Engrg* 2016;312:395–427.
- [14] Alessi Roberto, Vidoli Stefano, De Lorenzis Laura. A phenomenological approach to fatigue with a variational phase-field model: The one-dimensional case. *Eng Fract Mech* 2018;190:53–73.
- [15] Carrara P, Ambati M, Alessi R, De Lorenzis L. A framework to model the fatigue behavior of brittle materials based on a variational phase-field approach. *Comput Methods Appl Mech Engrg* 2020;361:112731.
- [16] Mesgarnejad A, Imanian A, Karma A. Phase-field models for fatigue crack growth. *Theor Appl Fract Mech* 2019;103:102282.
- [17] Ulloa Jacinto, Wambacq Jef, Alessi Roberto, Degrande Geert, François Stijn. Phase-field modeling of fatigue coupled to cyclic plasticity in an energetic formulation. *Comput Methods Appl Mech Engrg* 2021;373:113473.
- [18] Khalil Zeyad, Elghazouli Ahmed Y, Martínez-Pañeda Emilio. A generalised phase field model for fatigue crack growth in elastic–plastic solids with an efficient monolithic solver. *Comput Methods Appl Mech Engrg* 2022;388:114286.
- [19] Seleš Karlo, Aldakheel Fadi, Tonković Zdenko, Sorić Jurica, Wriggers Peter. A general phase-field model for fatigue failure in brittle and ductile solids. *Comput Mech* 2021;67(5):1431–52.
- [20] Seleš Karlo, Tomić Zoran, Tonković Zdenko. Microcrack propagation under monotonic and cyclic loading conditions using generalised phase-field formulation. *Eng Fract Mech* 2021;255:107973.
- [21] Seiler Martha, Linse Thomas, Hantschke Peter, Kästner Markus. An efficient phase-field model for fatigue fracture in ductile materials. *Eng Fract Mech* 2020;224:106807.
- [22] Seiler Martha, Keller Sören, Kashaev Nikolai, Klusemann Benjamin, Kästner Markus. Phase-field modelling for fatigue crack growth under laser-shock-peening-induced residual stresses. 2020.
- [23] Hasan Md Mehedi, Baxevanis Theocharis. A phase-field model for low-cycle fatigue of brittle materials. *Int J Fatigue* 2021;150:106297.
- [24] Golahmar Alireza, Kristensen Philip K, Niordson Christian F, Martínez-Pañeda Emilio. A phase field model for hydrogen-assisted fatigue. *Int J Fatigue* 2022;154:106521.
- [25] Simoes Marlini, Martínez-Pañeda Emilio. Phase field modelling of fracture and fatigue in shape memory alloys. *Comput Methods Appl Mech Engrg* 2021;373:113504.
- [26] Alessi Roberto, Ulloa Jacinto. Endowing griffith's fracture theory with the ability to describe fatigue cracks. *Eng Fract Mech* 2023;109048.
- [27] Loew Pascal J, Peters Bernhard, Beex Lars AA. Fatigue phase-field damage modeling of rubber using viscous dissipation: Crack nucleation and propagation. *Mech Mater* 2020;142:103282.
- [28] Schreiber Christoph, Müller Ralf, Kuhn Charlotte. Phase field simulation of fatigue crack propagation under complex load situations. *Arch Appl Mech* 2020.
- [29] Lo Yu-Sheng, Borden Michael J, Ravi-Chandar K, Landis Chad M. A phase-field model for fatigue crack growth. *J Mech Phys Solids* 2019;132:103684.
- [30] Havertho GA, Vale MG, Bittencourt ML, Boldrini JL. A non-isothermal thermodynamically consistent phase field model for damage, fracture and fatigue evolutions in elasto-plastic materials. *Comput Methods Appl Mech Engrg* 2020;364:112962.
- [31] Miehe Christian, Welschinger F, Hofacker M. Thermodynamically consistent phase-field models of fracture: Variational principles and multi-field FE implementations. 2010. p. 1273–311.
- [32] Ambati Marreddy, Gerasimov Tymofiy, De Lorenzis Laura. A review on phase-field models of brittle fracture and a new fast hybrid formulation. *Comput Mech* 2014;55(2):383–405.
- [33] Wu Jian-Ying, Nguyen Vinh Phu, Nguyen Chi Thanh, Sutula Danas, Sinaie Sina, Bordas Stéphane PA. Phase-field modeling of fracture. *Adv Appl Mech* 2020;53:1–183.
- [34] Freddi Francesco, Royer-Carfagni Gianni. Regularized variational theories of fracture: A unified approach. *J Mech Phys Solids* 2010;58(8):1154–74.
- [35] Cojocar Dan, Karlsson Anette. A simple numerical method of cycle jump for cyclically loaded structures. *Int J Fatigue* 2006;28:1677–89.
- [36] Tada Hiroshi, Paris Paul C, Irwin George R. The stress analysis of cracks. *Handbook Del Res Corp* 1973;34.
- [37] Suresh Subra. *Fatigue of Materials*. Cambridge University Press; 1998.
- [38] Dong Y, Garbatov Y, Guedes Soares C. A two-phase approach to estimate fatigue crack initiation and propagation lives of notched structural components. *Int J Fatigue* 2018;116:523–34.
- [39] Mughrabi Hael. Microstructural mechanisms of cyclic deformation, fatigue crack initiation and early crack growth. *Philos Trans R Soc Lond Ser A Math Phys Eng Sci* 2015;373. <http://dx.doi.org/10.1098/rsta.2014.0132>.
- [40] Smith James Ohrea. The effect of range of stress on the fatigue strength of metals. Technical report, University of Illinois at Urbana Champaign, College of Engineering ...; 1942.
- [41] Walker Kevin. The effect of stress ratio during crack propagation and fatigue for 2024-T3 and 7075-T6 aluminum. 1970.
- [42] Forman Royce G, Mettu SR. Behavior of surface and corner cracks subjected to tensile and bending loads in a Ti-6Al-4V alloy. 1992.
- [43] Ritchie RO, Davidson DL, Boyce BL, Campbell JP, Roder O. High-cycle fatigue of Ti-6Al-4V. *Fatigue Fract Eng Mater Struct* 1999;22(7):621–32.
- [44] Lovrich Neil Robert. *Fretting fatigue of Ti-6Al-4V: experimental characterization and simple design parameter* (Ph.D. thesis), Georgia Institute of Technology; 2004.
- [45] Strobl Michael, Seelig Thomas. On constitutive assumptions in phase field approaches to brittle fracture. *Procedia Struct Integr* 2016;2:3705–12.
- [46] Steinke Christian, Kaliske Michael. A phase-field crack model based on directional stress decomposition. *Comput Mech* 2019;63(5):1019–46.
- [47] Steinke Christian, Storm Johannes, Kaliske Michael. Energetically motivated crack orientation vector for phase-field fracture with a directional split. *Int J Fract* 2022;1–32.
- [48] Fan Meng, Jin Yan, Wick Thomas. A quasi-monolithic phase-field description for mixed-mode fracture using predictor–corrector mesh adaptivity. *Eng Comput* 2021;1–25.